Improved thermophysical characteristics of a new class of Ionic liquid + Diethylene Glycol/Al_2O_3+CuO based Ionanofluid as a coolant media for hybrid PV/T system.

Likhan Das[1,*], Navid Aslfattahi[2], Khairul Habib[1], R.Saidur [3,4], Kashif Irshad[5,6] Syed Mohd Yahya[7], Kumaran Kadirgama[8,9]

[1]Department of Mechanical Engineering, Faculty of Engineering, University of Malaya, Kuala Lumpur, 50603, Malaysia.

[2] Department of Fluid Mechanics and Thermodynamics, Faculty of Mechanical Engineering, Czech Technical University in Prague, Technická 4, 166 07 Prague, Czech Republic.

[3]Research Centre for Nanomaterials and Energy Technology (RCNMET), School of Engineering and Technology, Sunway University, 47500, Petaling Jaya, Malaysia.

[4]Department of Engineering, Lancaster University, Lancaster, LA1 4YW, UK.

[5]Interdisciplinary Research Center for Renewable Energy and Power Systems (IRC-REPS), King Fahd University of Petroleum & Minerals, Dhahran 31261, Saudi Arabia.

[6]Researcher at K.A.CARE Energy Research & Innovation Center at Dhahran, Saudi Arabia.

[7]Sustainable Energy and Acoustics Research Lab, Mechanical Engineering Department, Aligarh Muslim University, Aligarh 202002, India.

[8]Faculty of Mechanical and Automotive Engineering Technology, Universiti Malaysia Pahang, Pekan 26600, Malaysia

[9]Advanced Nano Coolant-Lubricant (ANCL) Lab, Automotive Engineering Centre, Universiti Malaysia Pahang, Pekan 26600, Malaysia

*Corresponding Author, Tel: + 8801849995964

E-mail: likhan.das11@gmail.com (Likhan Das); kumaran@ump.edu.my (Kumaran Kadirgama).

Abstract

The purpose of this experimental research is to develop a new class of nanofluid as a replacement of conventional water based nanofluid for medium temperature range as PV/T coolant application. For the first time, hybridized Al_2O_3+CuO nanoparticles were dispersed into the binary mixture of ionic liquid (IL) and diethylene glycol (DEG) without the addition of any stabilizing agents or surfactants. The formulated Ionanofluid posed excellent dispersion stability together with better thermal stability compared to water-based nanofluid, as evidenced from thermogravimetric analysis. The experimental thermal conductivity assessment showed a maximum of 41.8% enhancement together with a 31% penalty in pressure drop at 0.15 wt.% concentration. A hybrid PVT system is constructed to numerically examine the effect of Ionanofluid as an active cooling medium under the COMSOL Multiphysics environment. Ionanofluids as coolants in a PVT panel showed a maximum of 69% thermal efficiency at 0.15 wt.% Al_2O_3+CuO, higher than 63% (0.10 wt.% Al_2O_3+CuO), 58% (0.05 wt.% Al_2O_3+CuO), and 56% (pure IL+DEG). The PV panel temperature was reduced from 65 to 40 °C when IL+DEG was replaced with 0.15 wt% Al_2O_3+CuO. At the same concentrations, an electrical efficiency of nearly 12.7% was observed, representing a 29.91% improvement over IL+DEG at a flow rate of 4LPM. The formulated Ionanofluid performed thermally better than water but somewhat lower than water-based nanofluids like MWCNT/Water. Nevertheless, Ionanofluid's electrical efficiency was better than MWCNT/Water. Ionanofluid can be a viable alternative to water-based nanofluids for medium-temperature-based coolant applications.

Keywords: Ionic Liquid, PVT, electrical efficiency, thermal efficiency.

Nomenclature			
C_p	Specific heat (J/kg K)	Greek	
D	Diameter (m)	α	Absorptivity
DEG	Diethylene Glycol	ϕ	Concentration of Nanoparticles (wt%)
DSC	Differential Scanning Calorimeter	μ	Dynamic Viscosity (kg /m s)
[EMIM]	1-Ethyl-3-methylimidazolium	σ	Stefan's Boltzmann constant (W/m^{2}T^4)
EVA	Ethylene Vinyl Acetate	η	Efficiency

E	Energy Output (W/m^2)	ρ	Density (kg/m^3)
FTIR	Fourier transforms infrared	Subscripts	
G	Irradiance (W/m^2)	pv	Photovoltaic
h	Heat Transfer Coefficient (W/m^2 K)	eva	Ethylene Vinyl Acetate
IL	Ionic Liquid	ted	Tedlar
k	Thermal Conductivity (W/m K)	nf	Nanofluid
NP	Nanoparticle	bf	Base fluid
Nu	Nusselt Number	$conv$	Convection
Pr	Prandtl Number	rad	Radiation
PV	Photovoltaic	el	Electrical
PV/T	Photovoltaic Thermal	th	Thermal
Q	Heat Energy (W)	amb	Ambient
Re	Reynolds Number		
SEM	Scanning Electron Microscope		
[TF$_2$N]	Trifluoromethanesulfonimide		
T	Temperature (°C)		
TC	Thermal Conductivity		
TGA	Thermogravimetric Analysis		
UV	Ultraviolet		
UDF	User-Defined Fucntion		

1. Introduction

Governments are focusing on renewable energy sources and the development and expansion of the technology related to them as concerns about global warming, pollution, and rising energy demands, as well as the rising cost of fossil fuels and the looming threat of their depletion, are becoming more and more pressing (Nasrin & Hossain, 2021; Souza et al., 2022). The most common and accessible renewable energy source that can be used without harming the environment is solar energy. Solar energy photothermal conversion and utilization is the most popular and practical method of utilizing the sun's unbounded power. Photovoltaic thermal (PV/T) system is a crucial part of any solar thermal system because they take in solar radiation, transforming it into electrical energy for practical uses. The thermodynamic properties, such as thermal conductivity, specific heat, viscosity, and density, of the heat transfer fluid (HTF) play a crucial role in determining the overall efficiency of solar energy utilization (Liu et al., 2014). HTFs with superior thermodynamic properties and good thermal stability are highly desired for medium-to-high temperature solar applications, such as solar thermal power. Conventional water-based nanofluids cannot meet these requirements because they are thermally unstable at high temperatures. Therefore, the researchers' primary goal is to develop nanofluids that are both thermally and physically stable for medium to higher temperature PV/T applications.

PV/T technology was realistically proved for providing home electricity and heat demands by the partnership of IEC and Delmarva power and light business in 1973 and was displayed to the public. In light of this, several researchers and practicing engineers throughout the world continued to examine the commercial feasibility of this technology, and the results of their investigations have led to numerous design enhancements in PV/T technology. In the previous 50 years, a profusion of research and review publications about PV/T technology were published in the relevant literature, from which these design enhancements could be recognized. The electrical and thermal efficiency of PV/T systems, which are the critical characteristic of solar thermal energy systems, varies depending on the working fluid's properties and the geographical, climatic, and design conditions (Rubbi et al., 2021). In a PV panel, solar radiation is absorbed by the cells and the empty space between them, which raises the operating temperature of the system by absorbing energy not used by the solar cells. Although the efficiency of the cell increases as the radiation dose increases, the open-circuit voltage decreases, which also causes the efficiency of the cell as well as its operating temperature to decrease (Fayaz, Rahim, Hasanuzzaman, Rivai, et al., 2019; Sardarabadi & Passandideh-Fard, 2016). Many efforts have been made to lower the working temperature of PV panels in order to increase their electrical and thermal efficiency (Fayaz, Rahim, Hasanuzzaman, Nasrin, et al., 2019; Nahar et al., 2017; Nasrin & Parvin, 2012). In a nanofluid, nanometer-sized, very thermally conducive particles suspended in the base fluid produce a colloidal dispersion of nanoparticles in the base fluid. The use of nanofluids in solar heating systems as a working fluid is an attractive area of research for new and existing systems. Nanofluids may have significantly superior thermal properties to conventional fluids such as water, allowing for a significant increase in PVT system's electrical and thermal efficiency (Alous et al., 2019; Naghdbishi et al., 2020). As the volume of base fluid is significantly greater than that of nanoparticles, the characteristics of nanofluids will be dictated mostly by the properties of their base fluids. Water, ethylene glycol, refrigerant, or thermal oil are common examples of base fluids containing nanoparticle suspensions with diameters ranging from one nanometer to one hundred nanometers. Intermolecular interactions between liquid molecules and solid particles govern the formation of the interfacial layer in nanofluid suspension (Rajabpour et al., 2019). The selection of working fluids affects the density and viscosity of nanofluids. Ionic liquids have the capability of stabilizing filler nanoparticles by ionic solvation of the surface; thus, these structural changes are mirrored in the rheological characteristics of ionic liquids (Agafonov et al., 2022). Recent Ionanofluids with lower melting points (lower than 100 °C) exhibit better heat transfer coefficients than Ethylene glycol and water-based hybrid nanofluids due to their increased thermal conductivity viscosity at lower temperatures (Hu et al., 2021).In a study by (Minea & El-Maghlany, 2017), a numerical analysis conducted to assess the natural convection heat transfer utilizing Ionanofluids. A comparison of ionic liquid-based nanofluids and normal nanofluids reveals that adding modest volume concentrations of Al_2O_3 to the ionic liquid increases the Nusselt number significantly more than the water-based nanofluid. In another study, (Minea & Murshed, 2018) discovered inconsistent and contradictory behavior-changing the concentration of nanoparticles on the viscosity of Ionanofluids although most studies have seen an increase in the viscosity of INFs when adding nanoparticles to the base ionic liquid. However, ionic liquid-based nanofluids lack dispersion stability, which may be remedied by adding stabilizing agents such as surfactants (Bakthavatchalam et al., 2020). Contradictorily, using stabilizing agents deteriorate the thermophysical properties as evidenced in numerous studies (Al-Waeli et al., 2019). Therefore, the use of binary fluid as the base fluid becoming popular in formulating stable nanofluids other than formulating surfactant based nanofluid (Alkathiri et al., 2022; Yang et al., 2022). Metal-based, metal-oxide-based, carbon-based, and nanocomposites are all common types of nanoparticles. Researchers are presently exerting considerable effort to increase the thermal and electrical efficiency of PV/T systems by employing different nanofluids, in attempt to develop systems that are appealing to investors (Bretado-de los Rios et al., 2021). Various studies employing nanofluids as the PVT system's working fluid have demonstrated that they outperform traditional fluid-based systems in terms of thermal and electrical performance (Chaurasia & Sarviya, 2020; Varmira et al., 2021). (Nasrin, Rahim, et al., 2018) investigated a PV module under controlled conditions where a special thermal collector design, a full PVT system, and water/MWCNT nanofluid were used to enhance PV/T thermal performance. In their study, a 3D numerical simulation was corroborated at varying irradiation levels from 200 to 1000 W/m2, weight fraction from 0 to 1 % while maintaining mass flow rate 0.5 L/min and inlet temperature 32 °C. In numerical and experimental trials, nanofluid outperforms water by 4 and 3.67 %, respectively. The numerical and experimental overall efficiencies of a PV/T system with nanofluid and 1000 W/m2 irradiation are 89.2 and 87.65 %, respectively. The same research group conducted another investigation with water/MWCNT, which revealed that nanofluid assisted cooling improved tge PV electrical efficiency by 10.72 and 12.25%, respectively (Fayaz et al., 2018). The temperature of the solar cell decreases experimentally by 0.72 °C and numerically by 0.77 °C for every 10 L/h flow rate increase. Increases in flow rate of 10 L/h contribute 7.74 and 6.89 W of thermal energy, respectively, in theoretical and experimental studies. Water/MWCNT nanofluid improves PVT system thermal efficiency by 5.62 and 5.13 %, respectively, as compared to water. In another investigation, (Hasan et al., 2017) experimented with SiC, TiO_2, and SiO_2 nanomaterial nanoparticles to examine the PV/T unit's performance. Nanofluid was injected through 36 nozzles and four parallel tubes at the backside of the photovoltaic system. The SiC/H_2O nanofluid was reported to work optimally in the PV/T system, with a maximum electrical and thermal efficiency of 12.75 % recorded. (Motamedi et al., 2019) experimentally examined hydrophobic microchannels for PV/T devices using Ag–SiO_2 hybrid nanofluid and reported that the solar-thermal conversion efficiency and stagnation temperature and were increased by up to 20 % and 3 % respectively. Al_2O_3/water as a coolant nanofluid was used in a rectangular channel integrated with a silicon solar panel in a numerical study using the finite element method (FEM) to investigate the Navier-Stokes and energy equations. According to their findings, using nanofluid increased the rate at which heat was transferred from the panel to the fluid and thus improved system performance (Elmir et al., 2012). (Abdallah et al., 2018) used Al_2O_3/water nanofluid as a coolant in a PVT system in another study that used volume fractions of 0.2%, 0.1%, 0.5%, 0.3%, and 0.075 %. For the optimal outcomes, they concluded that the maximum efficiency occurred at a volume fraction 0.1%, which lower the panel temperature by 10°C at a flow rate of 1.2 L/min. In a recent study, (Hormozi Moghaddam & Karami, 2022) found the electrical and thermal efficiency was found higher using CNT based nanofluids while comparing with the Ag-MgO based nanofluid in a PVT system. Nevertheless, the frictional penalty encountered by CNT based nanofluid system was lower than that of Ag-MgO based nanofluids. Metal-oxide/water nanofluids as coolants in PVTs have been studied experimentally and computationally by (Sardarabadi & Passandideh-Fard, 2016). In their study, deionized water is used as a base fluid and Al_2O_3, TiO_2, ZnO as the nano dispersants at varying concentrations (0.05-10 wt.%). The electrical efficiency of TiO_2/water and ZnO/water nanofluids is superior to that of Al_2O_3/water nanofluid and deionized water, as noticed from both numerical and experimental results. In comparison to deionized water and the other two nanofluids, the ZnO/water nanofluid exhibits the highest thermal efficiency. Finally, the numerical model was used to investigate the effect of nanoparticles on the PV/T system's electrical and thermal performance and found that the thermal performance was nearly four-fold higher at the maximum of 0.10 wt.% than at 0.05 wt.%.

Although numerical and experimental investigations have shown that nanofluids considerably improve the performance of solar thermal systems, some significant challenges must be addressed before they can be considered a working fluid. Suspension stability of the nanofluids is the biggest technical challenge to overcome. Nanofluid stability can be affected by several factors, including the ratio of base fluid to NP and Np size, shape, and type. In contrast to other nanoparticles, metal-oxide-based NPs form noticeably more stable nanofluids due to the affinity between the base fluid and the metal oxide. TiO_2, Al_2O_3, ZnO, and CuO are just a few of the metal oxide nanoparticles that can be used to formulate nanofluids. To improve the stability of nanofluids, various mechanical (ultrasonication, mechanical shaking, magnetic stirring) and chemical techniques (surfactant addition, functionalization, pH control) are used. These strategies, however, have downsides of their own. Stabilizing agents, for example, cannot withstand high temperatures and lose effectiveness above a certain temperature threshold. Ultrasonication breaks down the structure of the NPs over time, deteriorating the thermophysical properties of the nanofluids. Furthermore, it was revealed that the additional cost of functionalizing nanofluids was futile. Ionic liquid (IL) appears as a viable alternative to conventional heat transfer fluid, capable of replacing surfactants in the preparation of nanofluids. Several recent studies with Ionanofluids (Ionic liquid-based nanofluid) showed excellent dispersion stability together with improved heat transfer performance in thermal systems (Main et al., 2021).

According to previous research, nanofluid-based PVT technology appears potential for solar-powered power generation. In contrast to water/surfactant-based nanofluids, however, there is a dearth of research on the formulation of Ionic Liquid/surfactant-free nanofluids for application in high-temperature-resistant PV/T systems. The objective of this research is to develop a nanofluid devoid of surfactants to prevent the detrimental thermophysical effects of surfactants. In addition, thermal feasibility difficulties with water as the base fluid at higher temperatures will be overcome by substituting a solution of IL+ Diethylene Glycol (DEG) for water, as it can sustain greater temperatures than water. The potential of core-shell nanoparticle-based nanofluids to increase thermal and electrical performance in a PV/T system will be examined and compared to that of conventional working fluid. To our knowledge, a binary solution of Glycol and ionic liquid has been employed as a substitute to the standard base fluid for the first time, which allowed the formulation of a stable nanofluid without the need of surfactants. The base fluid was made by mixing an ionic liquid ([EMIM] + [TF_2N]) with DEG, which are both hydrophobic in nature. The addition of IL improved dispersion stability while not compromising thermal stability. Metal oxide-based hybrid (Al_2O_3+CuO) nanoparticles (NPs) were used as nano dispersants at three different concentrations. The effects of nanoparticle concentrations on the thermophysical properties of Ionanofluid are discussed in this study. Finally, the performance of a PV/T system with this new class of Ionanofluid was evaluated and compared to that of base fluid alone.

2. Methods, preparation, and characterization

2.1. Preparation of [EMIM][TF_2N]+DEG/Al_2O_3+CuO Hybrid Ionanofluid

In this present work, the preparation of [EMIM][TF_2N] +DEG/Al_2O_3+CuO hybrid Ionanofluid was executed by two-step methods at 0.05, 0.10, and 0.15 wt% concentrations. The maximum concentration was chosen at 0.15 wt.% due to the fact that as the concentrations increased, observable sedimentation was seen, rendering the nanofluid unstable. CuO and Al_2O_3 nanoparticles that are employed in preparing hybrid nanoparticles are obtained from Us Research Nanomaterials, Inc. (Houston, TX, USA). The properties of NPs as per specifications of certificate analyses are shown in **Table 1**. Ionic liquid [EMIM] [Tf_2N] (CAS-No: 174899-82-2; ≥ 98% HPLC) and DEG were purchased from Sigma-Aldrich, Germany. The chemical structure of both components is shown in **Figure 1**. Engineering applications favour non-aqueous solvents such as [EMIM] [Tf_2N] because of their low vapor pressure, excellent thermal stability, strong conductivity, and wide applicable temperature range and electrochemical windows. Firstly, precisely weighted (using graduated cylinder) 30% of [EMIM][Tf_2N] was mixed with 70% of DEG by volume percentage to form an IL+DEG solution with a volume ratio of 30:70 (IL: DEG). A homogenous solution was obtained by carrying out two hours of stirring with a magnetic stirrer (IKA, RCT BASIC, Germany) for one hour at 1000 rpm and 60 °C temperature. To prepare the Ionanofluids sample, the precisely weighted Al_2O_3:CuO (1:1) NPs were distributed into the solutions at 0.05, 0.10 and 0.15 wt.% concentrations under continuous magnetic stirring at 800 rpm and 60 °C. It is worth noting that the Al_2O_3:CuO (1:1) mixing ratio was found to yield more stable nanofluids than the other experimentally trialled ratios (2:1, 1.5:1, 1:1.5, 1:2). As a result, Al_2O_3:CuO (1:1) was considered to produce Ionanofluid at various concentrations The samples of Ionanofluids were then stirred for two hours to improve the nanocomposite dispersion in the base fluid. To obtain a more stable Ionanofluid, each sample was sonicated for 4 hours with a power of 1200 W, 20 kHz ultra-sonicator (Ultrasonic Probe sonicator, Model: Fs-1200N, Hangzhou, China). Before being dispatched for characterization, the generated ionanofluids were cooled to room temperature spontaneously.

Table 1: Properties of nanoparticles.

Name	**Shape**	**Color**	**Average size (nm)**	**Purity**	**Specific surface area (m^2/g)**	**True Density (g/m^3)**
Al_2O_3	Nearly-spherical	White	60 nm	99.9%	58	3.89
CuO	Spherical	Brown-black	10 nm	99%	165	6.4

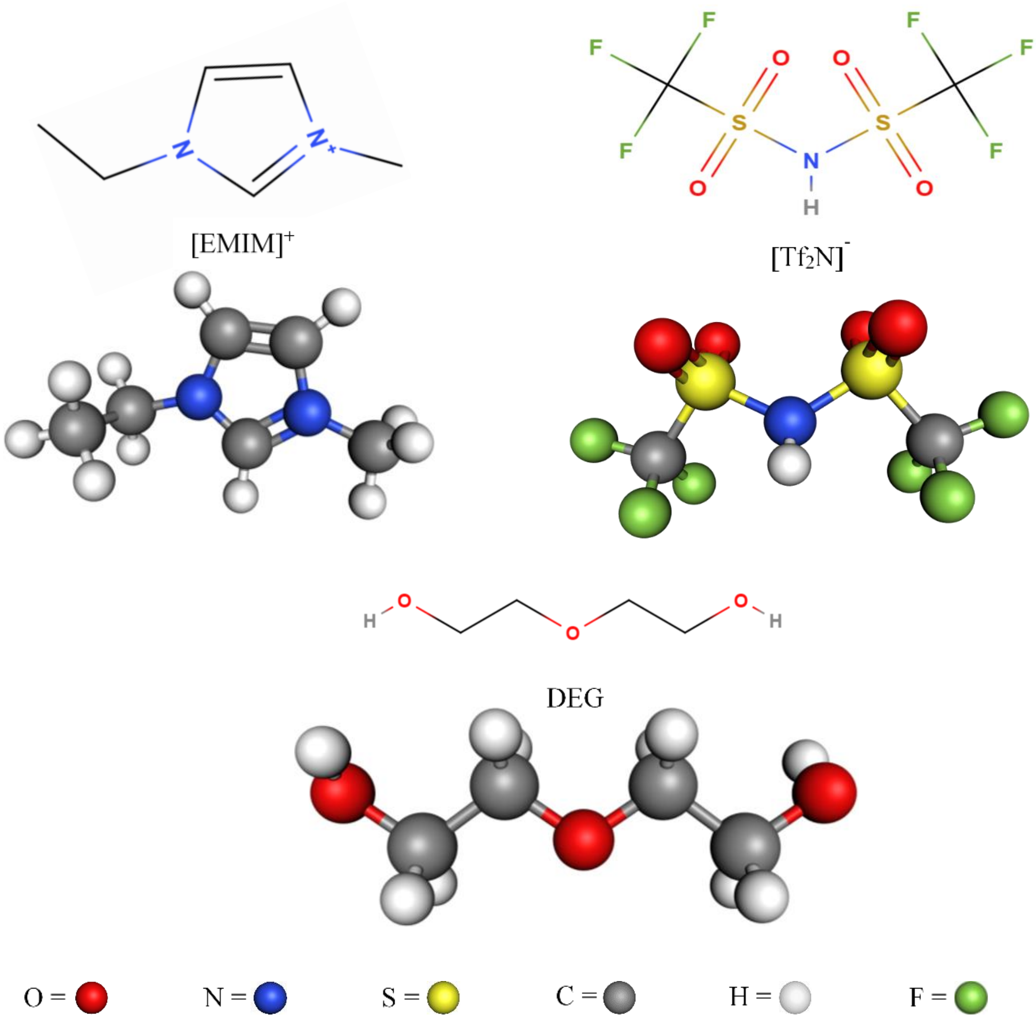

Figure 1. Chemical structure of [EMIM][Tf_2N] and DEG.

2.2. *Characterization*

2.2.1. Morphological and Optical Characteristics

The surface texture of the formed Al_2O_2+CuO nanoparticles was inspected with a scanning electron microscope (SEM). The operating voltage and current were 15 kV and 10 mA, respectively. Fourier transforms infrared (FTIR) spectroscopy was used to identify the chemical conformations of the formulated samples. The device was operated at a 0.2 scan speed for each spectrum while the resolution was set at 4 cm^{-1} resolution. The spectral wavelength ranged from 400 to 4000 cm^{-1}. The optical absorbance and transmittance were obtained by utilizing a UV-vis spectrometer.

2.2.2. *Zeta potential measurement*

The stability of colloidal solutions is directly related to the electrical potential in the interfacial double layer. The zeta potential is a widely used technique for determining the stability of nanofluids and colloidal solutions (Hunter, 2013). A particle analyzer (Litesizer-500, Anton Paar, Graz, Austria) was used to assess the zeta potential measurement of the prepared ionanofluids at different concentrations. For each sample, the measurements were taken at least three times to confirm the measurement accuracy.

2.2.3. Thermophysical Properties Measurements

The thermal conductivity (TC) measurement was accomplished by the transient hot-wire method employing a Tempos thermal property analyser as shown in **Figure 2**. The apparatus is capable of assessing TC values with an accuracy of 90% or higher. The sample was maintained at a constant temperature during the measurement by placing it in a constant temperature water bath. The sensed TC was converted into a digital signal and displayed on the monitor by dipping a single heated needle inside the sample, which served as a KS-3 sensor. As the sample temperature reached the anticipated value, the samples were left to equilibrate for at least 30 minutes before taking the measurement. Three readings were taken to check the repeatability at each point, and mean values were recorded to preserve measurement accuracy.

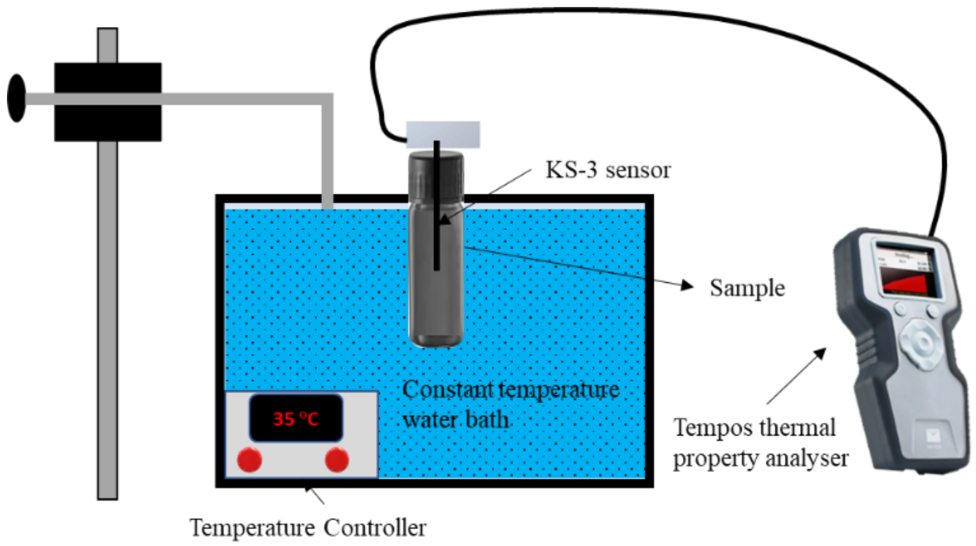

Figure 2. Schematic diagram of thermal conductivity measuring rig.

A differential scanning calorimeter (DSC) was involved to assess the specific heat capacity of the base IL+DEG and ionanofluids. A 40 μL aluminum crucible was used inside the apparatus in which samples were tightly sealed, and an N_2 atmosphere was accompanied by flowing N_2 at a 20 ml/min of flow rate. The heating rate was 10 °C/min, while the temperature ranged between 20–65 °C. The instruments had a temperature accuracy of ± 0.2 °C and exhibited a high resolution of 0.03 μW. The device was calibrated properly before measuring to ensure its sensibility and accuracy. However, the measurement uncertainty varied from 0.2–0.8%.

The viscosity and the shear property (shear stress and shear rate) were measured with a rheometer (MCR 92, Anton Paar, Austria). The measurement was assessed at 100 rpm with an accuracy of ± 1.0% in the temperature range of 20 to 60 °C. The density measuring device-densitometer (DMA-1001, Graz, Austria) has a 0.0001 g/cm^3 measuring accuracy. The water and air density tests were performed to ensure accurate measurement. The thermal stability was measured by performing TGA analyses with a TGA analyser (TGA 4000, Perkin Elmer, USA). The heating range was varied from 30–500 °C with a 10 °C/min heating rate inside a ceramic furnace while N_2 flowed at 1.9 bar and a rate of 19.78 ml/min.

2.3. Simulation Methodology

The simulation analysis yields the electrical and thermal characteristics of the PV/T system employing newly developed Ionanofluid. The methodology for simulating the PV/T system is detailed in the section that follows.

2.3.1. Physical System

Figure 3 depicts the problem under investigation. A large photovoltaic module with 72 polycrystalline silicon cells is considered in this study (each cell has an area of 0.024 m^2). According to the typical weather conditions in Malaysia, the average solar radiation is around 1000 W/m^2 (Mohammad et al., 2020). Therefore, the total area of the solar cells serves as the computational domain for numerical simulation (1.73 m^2). The physical properties of the layers in the PV/T module are shown in **Table 2**. The solar collector under research is a 300-watt photovoltaic module comprised of four layers: a photovoltaic solar cell, EVA on both sides of the photovoltaic cell, and a tedlar plate. In addition, a serpentine copper tubing heat exchanger is placed underneath the photovoltaic module (**Figure 3**). The PV cells, EVA, and tedlar layers are 0.3mm, 0.5mm, and 0.1mm thick. The remaining specifications are identical to those of the photovoltaic plate, i.e. (1955mm x 982mm).

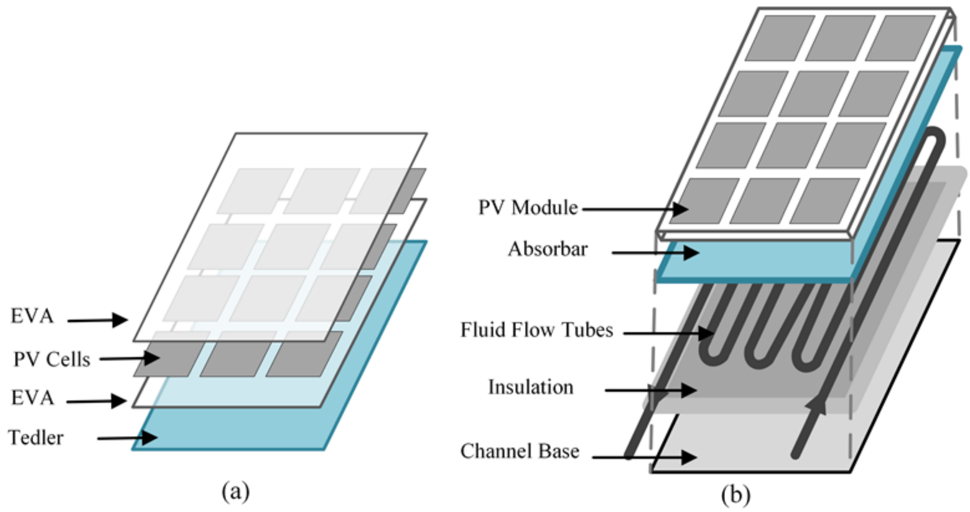

Figure 3. Schematic illustration of the backflow channel-based PV/T system with nanofluid as coolant (a) different layers (b) whole system.

Table 2: Specifications and properties of the hybrid PV/T system (Nasrin, Hasanuzzaman, et al., 2018a).

Parameter	**Values**
PV Material	Polycrystalline silicon cell
Power	300 W
Dimensions	1955 × 982 × 36 mm
Weight of PV panel	20.5 kg

Heat transfer coefficient inside PV layers, $h_{panel-ted}$	150 W/m^{2}K
Heat transfer coefficient from tedlar to heat exchanger, $h_{ted-tubing}$	77 W/m^{2}K
Heat transfer coefficient from heat exchanger to water/nanofluid, $h_{tubing-nf}$	66 W/m^{2}K
A_{PV}	0.9
A_{ted}	0.5
$Emissivity_{PV}$	0.99
k_{EVA}	0.311 W/m.K
k_{PV}	148 W/m.K
k_{Ted}	0.15 W/m.K
$k_{thermal\ paste}$	1.9 W/m.K
k_{tubes}	2700 W/m.K

2.3.2. Thermal modeling and governing equations

The Finite Element Method-based Multiphysics Software COMSOL is used to analyze numerical data. The output parameters of the PV/T system are determined using COMSOL's CFD and heat transfer modules. The flow of nanofluids is assumed to be steady, three-dimensional, incompressible, and laminar. The transmissivity of EVA is assumed to be approximately 100%, dust's effect on the absorptivity of the PV surface is negligible, and temperature variation along the module's thickness is assumed to be zero. Additionally, it is assumed that the base fluid contains a homogeneous mixture of nanoparticles (i.e., no particle sedimentation). In this study, base fluid and the hybrid Ionanofluid at varying nanoparticle concentrations are used. Regression analysis is used to fit the thermal conductivity, viscosity, and density, all related to the weight fraction at different temperatures, to a polynomial. This polynomial is then used in COMSOL through a user-defined function (UDF).

For solid domain in the PV/T device, heat conduction equations are used to account for heat transfer. Heat transmission from the surface of the photovoltaic panel to the flow channel is established using the heat conduction equation shown below in **Eq.1-4** (Samylingam et al., 2020).

$$\rho_c \delta_c C_{pc} \frac{\mathrm{d}T_c}{\mathrm{dt}} = \alpha_{panel} G - E_e - h_{panel-ted} - \left(T_{panel} - T_{ted}\right) + \left(k_c \delta_c \frac{\partial^2 T_c}{\partial x^2} + \frac{\partial^2 T_c}{\partial y^2} + \frac{\partial^2 T_c}{\partial z^2}\right) \tag{1}$$

Other equations of thermal energy for additional layers can be expressed similarly. Here, α_p represents the panel's absorptivity, G represents the irradiance, E_e stands for electrical energy output and $h_{panel-ted}$ expresses the heat transfer coefficient between PV module and tedlar plate. Correspondingly, other heat transfer coefficients between the layers are specified in **Eq.2** and **3**. Specifications of the PV/T collector are listed in **Table 2**.

From tedlar to serpentine tubing:

$$\rho_{ted} \delta_{ted} C_{p,ted} \frac{dT_{ted}}{dt} = -h_{panel-ted}\left(T_p - T_{td}\right) - h_{ted-tubing}\left(T_{ted} - T_{tubing}\right) + k_{ted} \delta_{ted} \left(\frac{\partial^2 T_{ted}}{\partial x^2} + \frac{\partial^2 T_{ted}}{\partial y^2} + \frac{\partial^2 T_{ted}}{\partial z^2}\right) \tag{2}$$

From serpentine tubing to nanofluid:

$$\rho_{ted} \delta_{tube} P dy C_{p,tube} \frac{dT_{tube}}{dt} = -h_{ted-tube}(T_{ted} - T_{tube}) - h_{tube-nf} P dy \left(T_{tube} - T_{nf}\right) + k_{tube} \delta_{tube} \left(\frac{\partial^2 T_{tube}}{\partial x^2} + \frac{\partial^2 T_{tube}}{\partial y^2} + \frac{\partial^2 T_{tube}}{\partial z^2}\right) \tag{3}$$

Where P is the periphery of the tube.

For working fluid in serpentine channel.

$$\rho_f A_f dy C_f \frac{dT_f}{dt} = h_{tube-nf} P dy (T_{tube} - T_{nf}) \tag{4}$$

Moreover, **Eqs.5-8** describes the mass and momentum and energy equations for steady laminar fluid flow.

$$\frac{\partial u}{\partial x} + \frac{\partial v}{\partial y} + \frac{\partial w}{\partial z} = 0 \tag{5}$$

X-momentum:

$$\rho_{nf} \left(u \frac{\partial u}{\partial x} + v \frac{\partial u}{\partial y} + w \frac{\partial u}{\partial z}\right) = \frac{-\partial P}{\partial x} + \mu_{nf} \left(\frac{\partial^2 u}{\partial x^2} + \frac{\partial^2 u}{\partial y^2} + \frac{\partial^2 u}{\partial z^2}\right) \tag{6}$$

Y-momentum:

$$\rho_{nf}\left(u\frac{\partial v}{\partial x}+v\frac{\partial v}{\partial y}+w\frac{\partial v}{\partial z}\right)=\frac{-\partial P}{\partial y}+\mu_{nf}\left(\frac{\partial^2 v}{\partial x^2}+\frac{\partial^2 v}{\partial y^2}+\frac{\partial^2 v}{\partial z^2}\right) \tag{7}$$

Z-momentum:

$$\rho_{nf}\left(u\frac{\partial w}{\partial x}+v\frac{\partial w}{\partial y}+w\frac{\partial w}{\partial z}\right)=\frac{-\partial P}{\partial z}+\mu_{nf}\left(\frac{\partial^2 w}{\partial x^2}+\frac{\partial^2 w}{\partial y^2}+\frac{\partial^2 w}{\partial z^2}\right) \tag{8}$$

The heat capacity (C_{Pnf}) of the nanofluid is considered to be constant, and their properties were obtained from the following correlation (Sardarabadi et al., 2014):

$$Cp_{nf}=(1-\phi)(C_P)_{bf}+\phi(C_P)_s \tag{9}$$

The Nusselt number for different flow regime between fluid and tube can be expressed as (Hendricks & van Sark, 2013).

Re < 2300, Nu=4.364

$$Re>2300,\quad Nu=0.0234\,Re^{0.8}Pr^{0.4} \tag{10}$$

In **Eq. 10**, Reynolds number Re and Prandtl Number Pr can be calculated as (Nasrin, Hasanuzzaman, et al., 2018a).

$$Re=\rho_f v_f D/\mu_f \tag{11}$$

$$Pr=\mu_f C_{pf}/K_f \tag{12}$$

Energy conservation is considered throughout the hybrid PV/T collector described in **Eq.13**, which includes solar irradiance, PV surface radiation, convection between the PV/T and the surrounding environment, thermal energy produced, and electrical power production.

$$G-P_{el}-P_{th}-Q_{conv}^{'}-Q_{rad}^{'}=0 \tag{13}$$

The following equations describe the convection and radiation heat transport from a PV/T device. The panel's radiative and convective heat transfer coefficients are determined using Stefan-Boltzmann laws and Newton's cooling, respectively.

$$-n.(-k\nabla T)=h_{total}\left(T_{surface}-T_{ambient}\right) \tag{14}$$

$$-n.(-k\nabla T) = \varepsilon\sigma\left(T_{surface}^4 - T_{sky}^4\right) \tag{15}$$

Where, h_{total} denotes the total heat transfer coefficient expressed in terms of $h_{total} = \left(h_{forced}^3 + h_{natural}^3\right)^{\frac{1}{3}}$. This involves both natural and induced convection effects over the panel. The coefficients of forced and natural convection heat transfer (Hendricks & van Sark, 2013) are determined using **Eqs.16** and **17**.

$$h_{natural} = 1.78\left(T_{amb} + T_{surface}\right)^{\frac{1}{3}} \tag{16}$$

$$h_{forced} = 2.8 + 3.0V_{wind} \tag{17}$$

While sky temperature is determined using the Swinbank relation (Nasrin, Hasanuzzaman, et al., 2018b) as $T_{sky} = 0.037536T_{amb}^4 + 0.32T_{amb}$. **In Eq.15**, ε is the emissivity and σ denotes the Stefan-Boltzmann constant.

Where, ρ and V is the density and velocity of the fluid, respectively. D is the diameter of the tubes of the thermal collector.

The output thermal energy is calculated by:

$$P_{th} = mC_p(T_{out} - T_{in}) \tag{18}$$

Eq.17 determine the thermal efficiency.

$$\eta_{th} = \frac{P_{th}}{G \times A_c} \tag{19}$$

2.3.3. Electrical modeling of PV panel in Simulink

The systematic block diagram of a PVT co-generation system is shown in **Figure 4**a. Metallic copper tubes are linked to the rear of PV panels through which nanofluid will flow to reduce panel temperature. The panel's output is sent to the DC-AC converter through an MPPT/DC-DC converter. The inverter's obtained alternating current output is sent to the grid or an electrical load. Simultaneously, heat recovered from the PV panel via circulating fluid will be used as supplementary heat energy by the thermal power plant to generate electrical energy. On the electrical side, the system's efficiency can be boosted by boosting the efficiency of the panel-MPPT system and inverter system.

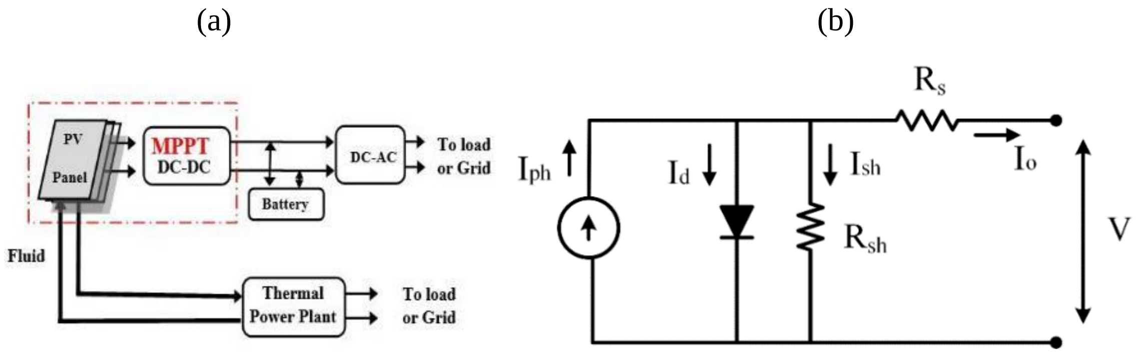

Figure 4. (a) Schematic of the PVT co-generation system. (b) equivalent model of a solar PV cell.

The model of the PV panel is developed using the model of the single PV cell. The ideal solar cell acts as a current source connected with a diode in the parallel connection. A very common solar cell equivalent circuit is shown in **Figure 4**b, consisting of a current source, a diode, and resistors. One resistor is series-connected, and one is in parallel connection. The expressions for the various parameters of the solar cell used to develop PV panel model are described below (Arif et al., 2018):

Module Reverse saturation current can be expressed as,

$$I_{rr} = I_{SCR} \Big/ \left[e^{\left(q.\frac{V_{oc}}{K}.N_S.A.T_{rk}\right)} - 1 \right] \tag{20}$$

PV module saturation current is expressed by,

$$I_d = I_{rr} \times \left(T_{aK} / T_{rK} \right) \times e^{\left[\left(E_g \times \frac{q}{k} \times A\right) \times \left(\frac{1}{T_{rk}} - \frac{1}{T_{aK}}\right) \right]} \tag{21}$$

Light generated current can be expressed as,

$$I_{PV} = [I_{SCR} + K_i \times (T_{aK} - T_{rk}) \times \frac{S}{1000} \tag{22}$$

And the expression for Output current,

$$I_o = N_P \times I_{PV} - N_P \times I_d \left[e^{\left[\frac{q}{Ns} \times A \times K \times T_{aK}\right) \times (V_o + I_o R_s)]} - 1 \right] \tag{23}$$

The basic building block of a PV array is the PV cell. PV cells are grouped together in a series and parallel fashion to make a PV module that makes the PV array. The modeling of a single PV cell is described using various fundamental equations. The equivalent electric circuits of the PV cell and PV array are shown below in **Figure 5**a, and **Figure 5**b, respectively. The current source

I_{ph} represent the cell photocurrent and is the actual current produced due to the sunlight. R_{sh} and R_s are the intrinsic shunt and series resistance which incorporate the actual behavior of the cell.

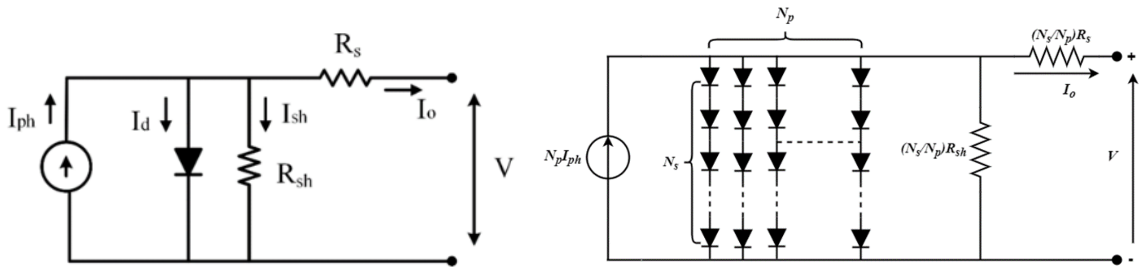

Figure 5. Equivalent Circuits of (a) PV Cell and (b) PV Array.

The following equation determines the V-I characteristic equation of the cell,

$$I_{ph} = [I_{sc} + K_i(T - 298)] \times \frac{I_r}{1000} \tag{24}$$

Here, I_{ph} is the photocurrent generated by one cell in Ampere (A), I_{sc} is the short-circuit current (A). K_i is the short circuit current of a single cell at 1000 W/m^2 and 25°C; I_r is the solar irradiation in W/m^2. Similarly, the reverse saturation current I_{rs} can be determined as

$$I_{rs} = \frac{I_{sc}}{e^{\left(\frac{qV_{oc}}{N_s BnT}\right)-1}} \tag{25}$$

Where I_{sc} is the short circuit current (A), q is the charge of an electron, N_s is the number of cells connected in series, V_{oc} is the open circuit output voltage, B is the Boltzmann constant, and n is the ideality factor of the diode. The module saturation current I_s vary according to the following equation,

$$I_s = I_{rs}\left[\frac{T}{T_r}\right]^3 exp\left[\frac{qE_{g0}}{nB}\left(\frac{1}{T} - \frac{1}{T_r}\right)\right] \tag{26}$$

Where E_{g0} is the energy band-gap of the material used as semiconductor, and T_r is the nominal temperature (298.15 K). The module's current output is calculated using the equation given below,

$$I_o = N_p I_{ph} - N_p I_s \left[exp\left(\frac{\frac{V}{N_s} + \frac{I_o R_s}{N_p}}{nV_t}\right) - 1\right] - I_{sh} \tag{27}$$

With $V_t = \frac{kT}{q}$and $I_{sh} = \frac{\frac{VN_p}{N_s} + I_o R_s}{R_{sh}}$.

A model of the solar cell is developed using these equations in MATLAB/Simulink. Series and parallel combination of these cells gives us the PV panel model having required output power. The specifications for the single PV panel developed are tabulated in **Table 2**.The output electrical is calculated by:

$$P_{el} = V_{oc} \times I_{sc} \times FF \tag{28}$$

Eq.29 is used to determine the electrical efficiency.

$$\eta_{el} = \frac{P_{el}}{G \times A_c} \tag{29}$$

Where, G is the effective irradiance taking into consideration absorptivity, transmissivity and packing factor of the solar module.

2.3.4. Boundary Condition

Throughout the domain, proper boundary conditions were employed in accordance with the physics of the problem. The boundary condition that is applied across the top and bottom layers of the photovoltaic module is $-\boldsymbol{n}.q = h_c(T_{amb} - T_s)$. Where **n** is the surface normal and T_{amb} and T_s are the surrounding environment and surface temperatures, correspondingly. The boundary conditions are summarized in **Table 3**.

Table 3. Summary of boundary conditions.

Domain	Boundary condition	Expression
Fluid domain	Velocity Inlet along x-axis	$u = U_0, v = 0, w = 0 \; and \; T = T_0$
Solid Domain	No-slip conditions	$u = v = w = 0$
Solid-fluid Interfaces	Heat flux continuity	$\left(\frac{\partial T_s}{\partial n}\right)_f = \frac{k_s}{k_f}\left(\frac{\partial T_s}{\partial n}\right)_s$
Fluid Outlet	Zero Pressure outlet	$P = 0$
Solid Walls	adiabatic boundary	
Bottommost plate	Isolated Boundary	

2.3.5. Meshing and Grid independence

COMSOL Multiphysics® was used to mesh the PV/T module using the physics-controlled mesh sequence configuration, as illustrated in **Figure 6**(a-c). Each domain and boundary have its own tetrahedral and triangular mesh elements. The number of mesh elements at each boundary rises in order to heat transfer and flow fields can be effectively modeled.

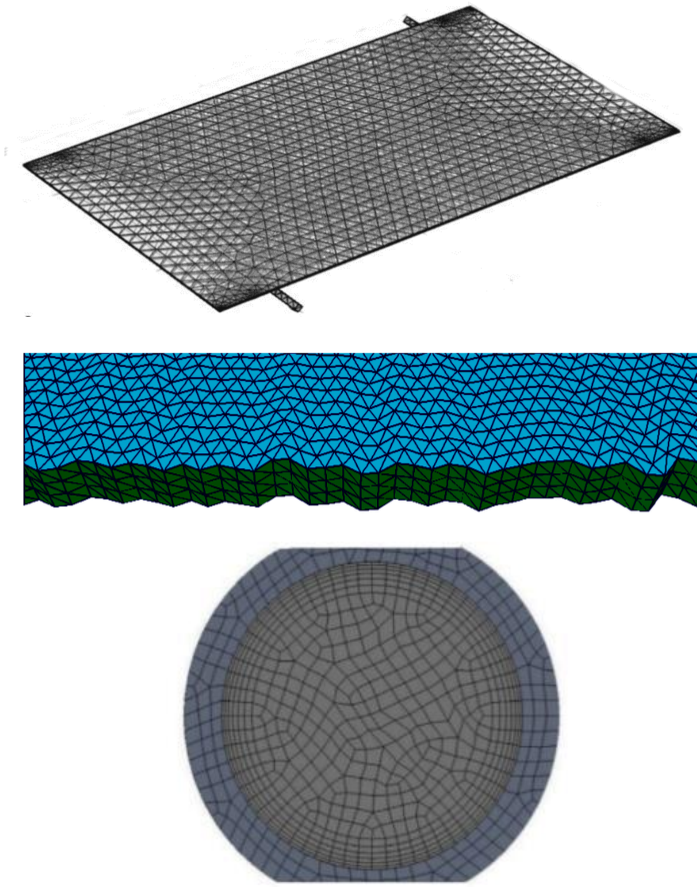

(a)

(b)

(c)

Figure 6. Finite element meshing (a) PV/T collector (b) along the thickness of the collector (c) inner and outer portions of the tube.

The mesh convergence criterion was obtained by performing simulation at a mass flow rate of 3 LPM and solar irradiance of 1000 W/m^2 using water with different mesh sizes (from coarser to finer) shown in **Table 4**. The initial layer thickness was set to 1/50 of the element's size at that boundary. The output of grid convergency is presented in **Figure 6**(b-c) at different mesh sizes. It is obvious from the table there was no further change in panel temperature, and outlet fluid temperature values after element size reached to1.5×10^6. Thus, an element size of 1.5×10^6 was preferred for simulation purposes. The solution method of the governing equations using COMSOL Multiphysics modelling package is shown in **Figure 7** below via flowchart:

Table 4. Grid independence test.

S. No.	**Mesh size (elements)**	**PV Temp. (℃)**	**Deviation (%)**	**Outlet Temp. (℃)**	**Deviation (%)**	**Solution Time (s)**
1	2.5×10^{5}	42.341	--	41.213	--	560
2	4×10^{5}	43.872	1.2%	40.751	-1.13%	720
3	6×10^{5}	44.003	0.29%	40.254	-1.23%	817
4	8×10^{5}	44.118	0.26%	39.104	-2.94%	1115
5	1.5×10^{6}	45.200	2.3%	38.889	-0.55%	1487
6	3.5×10^{6}	45.201	0.002%	38.801	-0.22%	1815

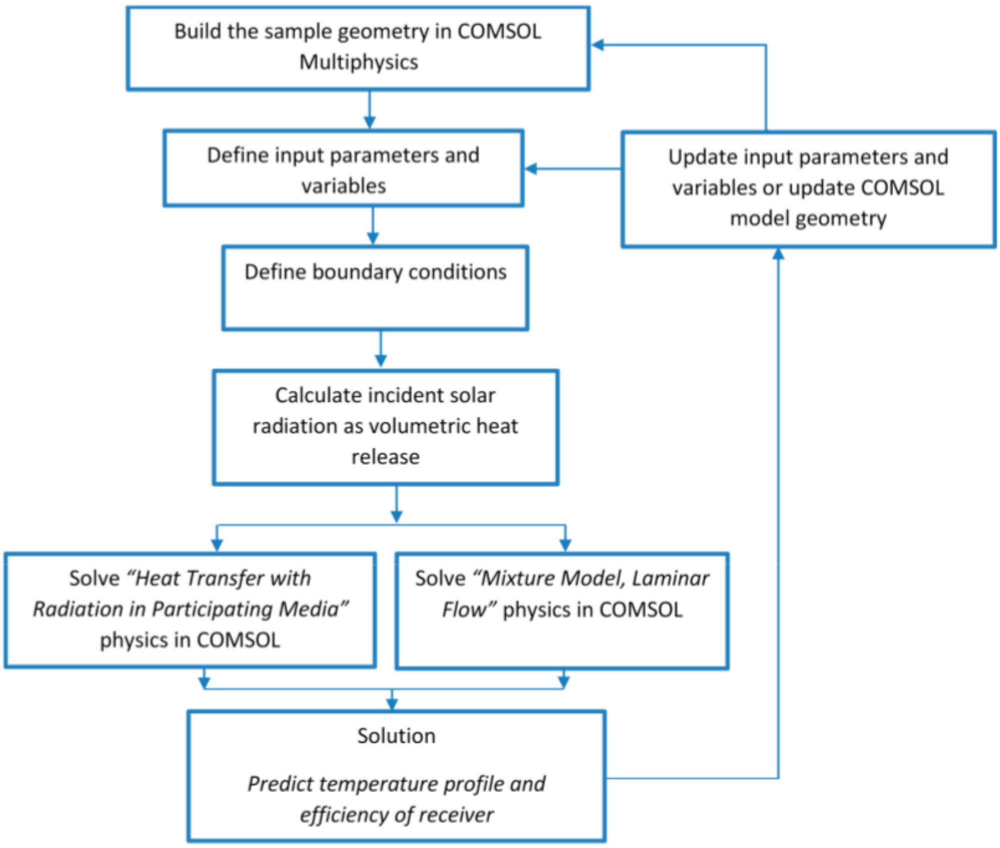

Figure 7. Flowchart representing the methodology in COMSOL environment.

3. Results and Discussion

3.1. SEM Analysis

The SEM analysis was conducted to confirm the surface morphology of the nanoparticles under investigation. It is obvious from the micrographs (**Figure 8**a**)** that the utilized Al_2O_3 is spherical with a combination of α (~60%) and (~40) γ characteristics. The size distribution plot also reports that the diameter of most of the particles stays in the range of 55-70 nm (**Figure 8**b**)**. Furthermore, according to the SEM photographs of the CuO nanoparticles (**Figure 8**c**)**, the shape of the particles is nearly spherical, with 75% of them being sized between 7–12 nm (**Figure 8**d**)**. The information from the SEM micrographs strongly supports the "product description" provided by the supplier. Moreover, the SEM micrographs are aligned with the findings from previous studies for Al_2O_3 (Mei et al., 2018) and CuO (Bonnot et al., 2015) NPs, respectively.

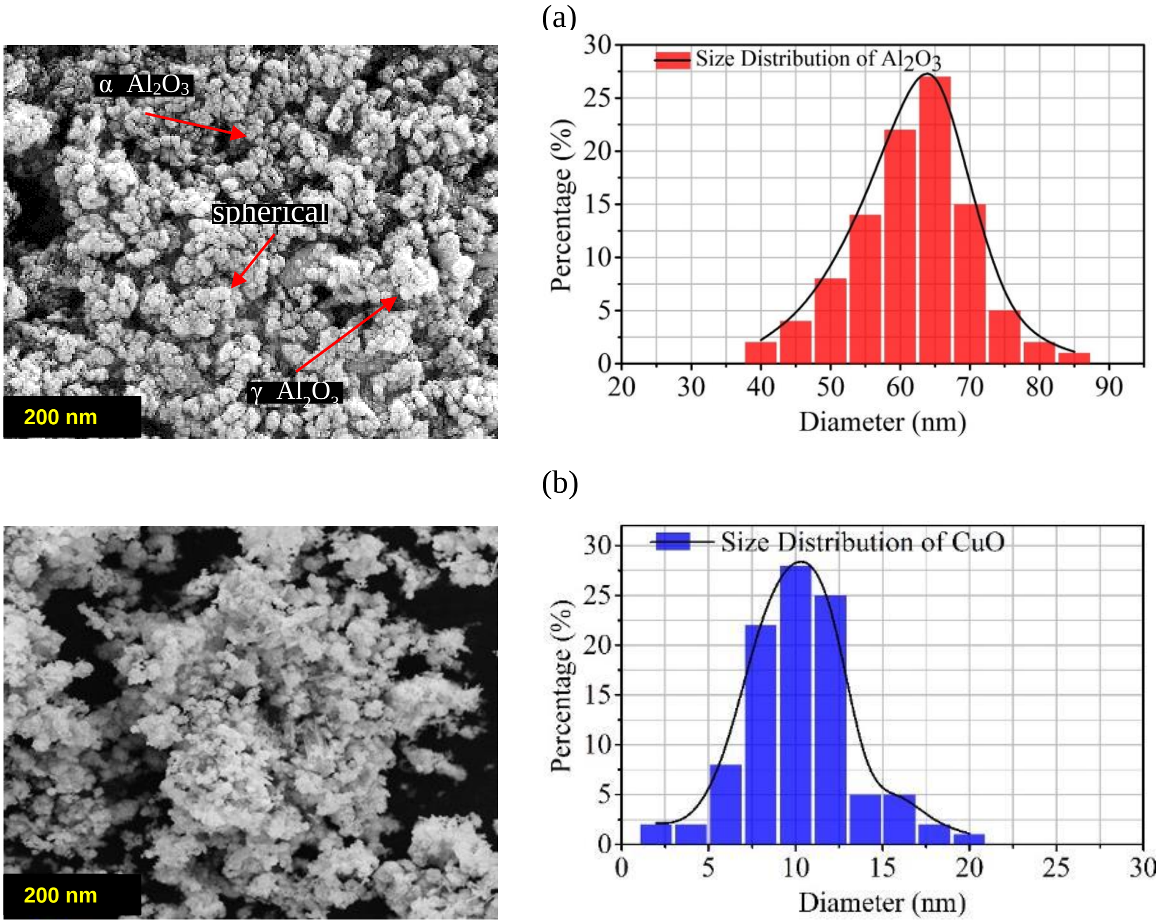

Figure 8. SEM micrograph and particle size distribution of (a)Al_2O_3, (b) CuO nanoparticles.

3.2. *Stability Analysis*

The most challenging part of synthesizing nanofluids is maintaining the stability of the formulated nanofluids. The suspended nanoparticles in the base fluids are prone to sedimentation resulting from the effect of various forces acting on them, such as Van der Waal forces, electrostatic repulsion, and to some extent, buoyancy and gravitational forces. According to the DLVO theory, nanofluid instability, causing the agglomeration of the suspended nanoparticles, is attributed to the domination of the Van der Waal attraction force over the electrostatic repulsive force. Therefore, care must be taken during the formulation of nanofluids to ensure the stability of the nanofluid. Different approaches can be adopted to improve stability, as depicted in **Figure 9**a. Among these techniques, the pH adjustment and the surfactant additions have some demerits. For instance, increasing or decreasing pH can increase the alkalinity or acidity, which detrimentally affects the pipes by causing corrosion, fouling, etc. However, adding surfactants reduces thermal stability because most surfactants cannot withstand temperatures above 60 °C. Furthermore, the addition of stabilizing agents deteriorates the desired thermophysical properties.

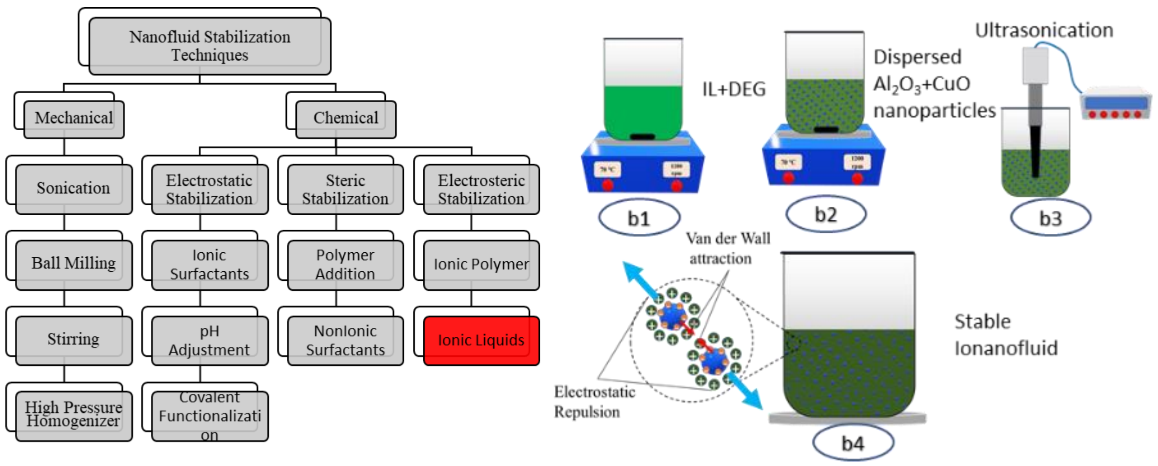

Figure 9. (a) Nanofluid stabilization techniques (Chakraborty & Panigrahi, 2020) (b) approaches to tune the Ionanofluid stability using an Ionic liquid, (b1) preparing the homogenous mixture of IL+DEG by hot plate magnetic stirring, (b2) dispersion of nanoparticles into the base fluid by hot plate magnetic stirring, (b3) ultrasonication using probe ultra-sonicator (b4) formulation of stable Ionanofluid

Mechanical approaches are emphasized in this study to achieve the desired stability, as well as the addition of an ionic liquid in a moderate ratio (IL: DEG = 20: 80) to achieve electrostatic stabilization by increasing the double layer repulsive force with a modified particle surface, as shown in **Figure 9**b. The measured values of the ζ potential are plotted in **Figure 10**a for different concentrations of nanoparticles. The presence of IL provides electrostatic repulsive forces that make the solutions highly stable, as demonstrated by the ζ potential value that ranged between -60.8mV to -45.3mV. Furthermore, the ionanofluids are more stabilized by fluid agitation and cavitation due to the ultrasonic waves. When the number of nanoparticles is increased, more repulsive forces between the IL ions and the nanoparticles are generated, causing the ζ potential to rise. The visual inspection of nanofluids revealed that no precipitation formed after two weeks (**Figure 10**b), indicating that these ionanofluids could be an excellent choice for solar energy storage applications.

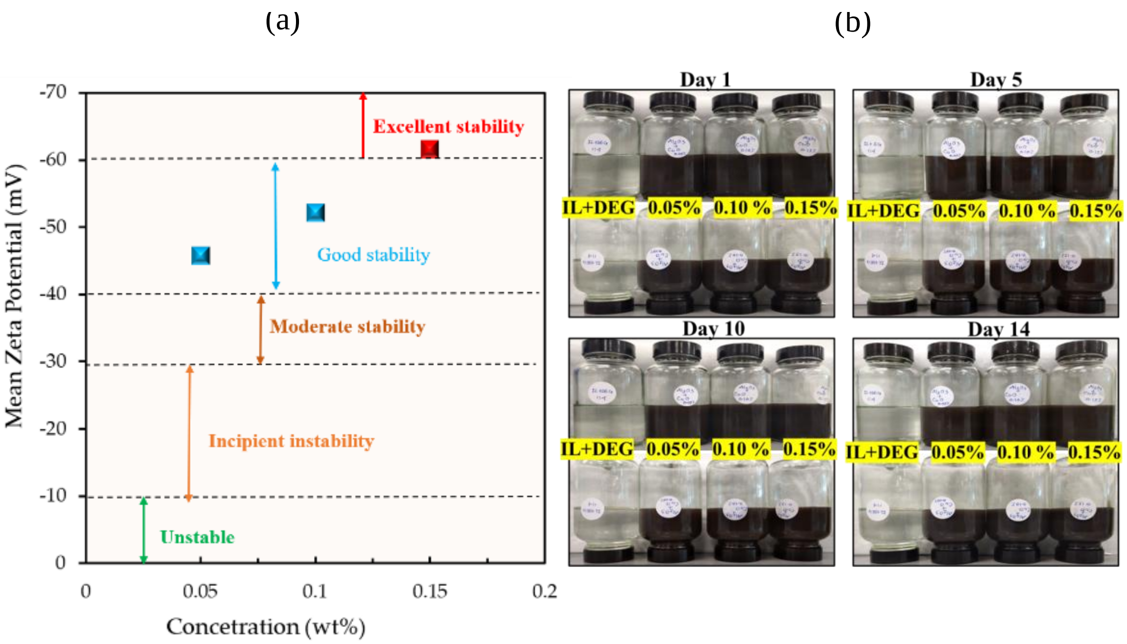

Figure 10. (a) Mean Zeta potential vs concentration, (b) Digital photograph of the formulated IL+DEG/Al_2O_3+CuO hybrid Ionanofluid at different concentrations from day1 to day14.

3.3. *FTIR Analysis*

Figure 11 shows the identified IR spectra for DEG+IL and ionanofluids for wavelengths ranging from 4000-600 cm^{-1}. Chemical bonds have been assigned to the transmittance peaks at various wavenumbers, as shown in **Table 5**. The stretching O-H bond induces the broad peak at 3352 cm^{-1}, while the aliphatic C-H stretching of DEG generates the broad peak at 2873 and 2895 cm^{-1} (Saikia et al., 2017). The IL contents, on the other hand, contribute to the appearance of several peaks at 1572 and 1351 cm^{-1}, which are attributed to the stretching C=N, and C-C bonds, respectively, while the stretching S-O and C-F bonds are responsible for the observed peaks at 1053 and 1190 cm^{-1}, respectively (Abdollahi et al., 2018). A vibrating C=C bond in IL's aromatic cationic aromatic compound also accounts for the strong peak at 893 cm^{-1}. It's worth noting that the insignificant addition of nanoparticles had no chemical reaction with the molecules of the base fluid, as the FTIR of pure IL+DEG and Ionanofluid showed no significant differences.

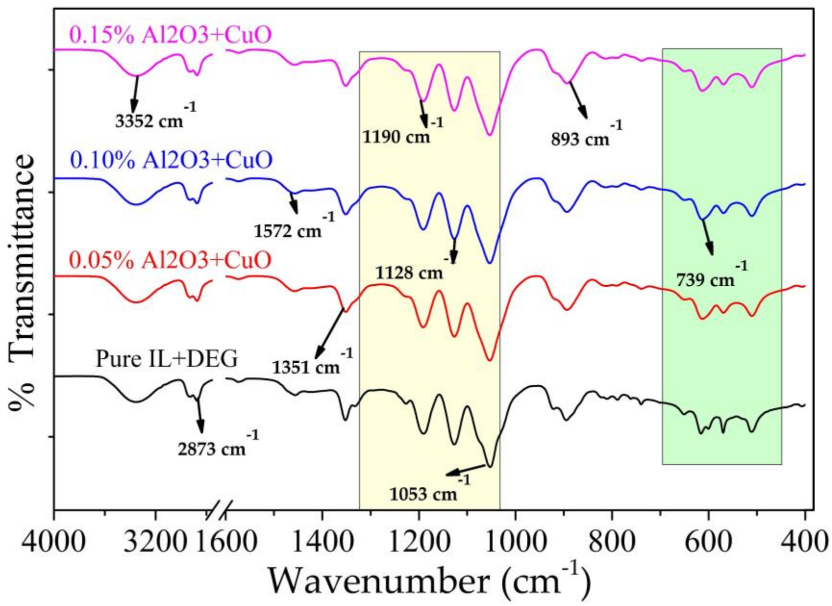

Figure 11. FTIR spectra of Pure IL+ DEG and IL+DEG/ (Al_2O_3+CuO) nanofluids at different concentrations.

Table 5. Assigned Chemical bonds of the peaks of FTIR bands of IL+DEG and Ionanofluid.

Peaks	**Type**	**Assignments**
3352	Strong, broad	O-H stretching
2873	Strong sharp	C-H stretching
1351	Strong	C-N stretching
1190	Strong	C-F stretching
1128	Strong	C-F stretching
1053	Strong	S-O stretching
893	Strong	C=C bending
739	Strong	C-H bending

3.4. UV-Vis Analysis

Figure 12a and **Figure 12**b depict the absorbance and transmittance spectra of pure IL+DEG and Ionanofluids for wavelengths ranging from 800 to 200 nm, respectively. Due to both constituents' poor optical absorption properties, the mixture of [EMIM][Tf_2N] and DEG exhibits high transmittance and low absorbance in the visible wavelength. When Al_2O_3+CuO nanoparticles are dispersed in the base fluid, they significantly increase light-absorbing properties while simultaneously losing optical transmittance. The improved absorptivity of Ionanofluids explains the high potential of hybrid nanoparticles (Al_2O_3+CuO) in capturing solar light. The absorbance increases significantly in the wavelength range between 250 and 800 nm as the concentration of nanoparticles increases from 0.05 to 0.10 wt.%, and the transmittance of Ionanofluids completely disappears. However, from 200 to 600 nm, at a concentration of 0.15 wt.%, the absorbance is almost identical to that of 0.10 wt.%.

Nonetheless, the absorption property of Ionanofluids increases with the addition of nanoparticles at wavelengths greater than 600 nm. The higher the absorption capability, the better the solar conversion efficiency, implying that the added nanoparticles will significantly improve energy storage capability. Because the phenomenon of losing thermophysical and optical properties is common for nanofluids, it is critical to investigate the sustainability of the optical properties with time to assess the applicability of Ionanofluids. **Figure S1(a-e)** illustrates the variation in absorbance and transmittance spectra as a function of time. No significant shifts in absorbance or transmittance lines can be seen, indicating that the formulated Ionanofluid maintains its light-capturing ability over time.

(a) (b)

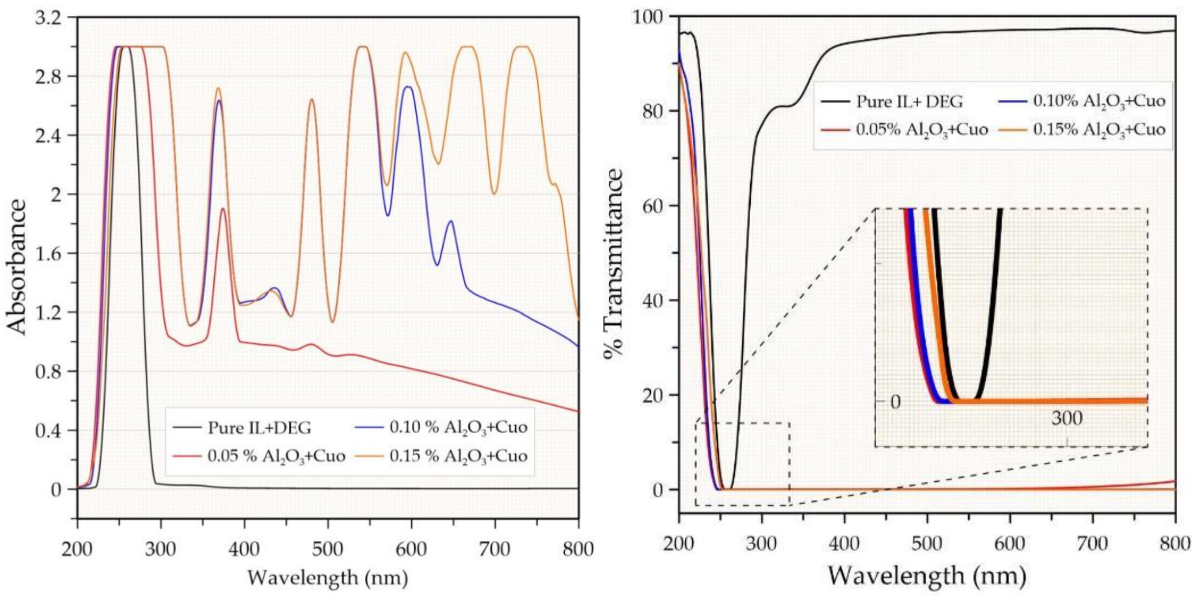

Figure 12. UV-Vis (a) absorbance and (b) transmittance spectra of pure IL+DEG and IL+DEG/Al_2O_3+CuO nanofluids at different nanoparticle loadings.

3.5. Thermal Conductivity

Figure 13a displays the TC vs. temperature plot of [EMIM][Tf_2N], DEG, base fluid (IL+DEG), and Ionanofluids at different concentrations in the temperature range of 20–80 °C. For each measurement, the measurement uncertainty was less than 5%. The TC of pure [EMIM] [Tf_2N] was observed to decrease slightly with increasing temperature, which is consistent with the findings of (Ge et al., 2007). Nonetheless, the trend lines for DEG and formulated nanofluids increased as the temperature increased. Rising TC as temperature increases is common in nanofluids and can be explained by some well-known concepts. The interfacial thermal resistance between the solid NPs and the base fluid is reduced by adding nanoparticles, increasing the TC as the temperature rises. However, at different concentrations of nanofluids, the rise in thermal conductivity tends to be linear with the temperature increase. In addition, nanoparticle concentration plays a vital role in the thermal behavior of the formulated nanofluids. The tendency for the TC to increase with increasing nanoparticle loading until it reaches an optimum concentration is typically obvious for nanofluids. The thermal conductivity decreases as the interaction between NPs and fluid molecules break down above this optimum concentration. Furthermore, sedimentation and agglomeration of nanoparticles at high concentrations are also attributable to the deterioration of the TC enhancement rate. In this present study, the formulated hybrid Ionanofluids experienced an increase in the TC for all three concentrations of 0.05, 0.10, and 0.10 wt%. This is attributable to the fine dispersion of highly conductive solid particles into the base fluids. The thermal conductivity ratio (TCR) of hybrid Ionanofluids is illustrated in **Figure 13**b. As seen from the figure, the maximum 41.8% enhancement in thermal conductivity occurs at 80 °C for the maximum nanoparticle concentrations of 0.15% regarding IL+DEG, 28% higher than pure DEG.

In some earlier investigations, the Al_2O_3-CuO nanoparticle pair was dispersed with several to assess the enhancement of the TC at different nanoparticle concentrations. The summary of these studies is listed in **Table 6**, and they are compared with the findings of this present study. To the best of the author's knowledge, none of these formulated hybrid Al_2O_3-CuO based nanofluids are suitable for applications in the medium to higher temperature range because the base fluid used in these nanofluids has low thermal stability or the surfactants used in these nanofluids cannot withstand temperatures above 60 °C. As a result, the current research focuses on developing a surfactant-free nanofluid with a wider temperature range of application. When comparing our findings to previous research, it's worth noting that the increases in TC in this study are more significant due to the strong synergistic effect of IL+DEG and NPs. Surfactants also degrade the thermal properties of solid nanoparticles by increasing thermal resistance when layered on the surface. As a result, the thermal resistance of surfactant-free nanofluids is lower than that of surfactant-containing nanofluids.

Table 6. Comparison of TC enhancements between glycol/water-based nanofluids with Al_2O_3-CuO nanoparticle pair.

Base fluid	**Conc.**	**Method**	**Surfactant**	**Stability**	**Maximum *k* enhancement**	**Ref**
[EMIM] [Tf_2N]+DEG	0.05-0.15 wt%	Two-step	-	Good-Excellent	41.8%	This work
Water + EG	1.0 vol %	Two-step	LAS	Moderate	12.33%	(Wanatasanappan et al., 2020)
Water + PG	0 - 3.5 vol%	Two-step	-	Moderate	~ 41 %	(Kumar & Sahoo, 2019)
Water	0.05 – 0.2 vol%	Two-step	-	-	9.7%	(Senthilraja et al., 2015)

Some well-established classical models were developed to predict the TC of nanofluids. For instance, the Maxwell and Hamilton-Crosser (H-C) models gained immense popularity for predicting the TC of different nanofluids. **Eq.30** is the expression for the thermal conductivity ratio by Maxwell models, while **Eq.31** stands for thermal conductivity ratio by (H-C) model.

$$\frac{k_{nf}}{k_{bf}} = \frac{k_{np} + 2k_{bf} - 2(k_{bf} - k_{np})\varphi}{k_{np} + 2k_{bf} + (k_{bf} - k_{np})\varphi} \qquad (30)$$

$$\frac{k_{nf}}{k_{bf}} = \frac{k_{np} + (n-1)k_{bf} - (n-1)(k_{bf} - k_{np})\varphi}{k_{np} + (n-1)k_{bf} + (k_{bf} - k_{np})\varphi} \qquad (31)$$

Here, k_{nf}, k_{bf}, k_{np}, and φ are thermal conductivity of the nanofluid, base fluid, nanoparticles, and nanoparticles concentration, respectively. However, these models often fail to provide a precise prediction because several variables such as temperature, nanofluid types, concentrations, size and the shape of nanoparticles are needed to be considered for accurate predictions. Therefore, developing empirical correlations based on experimental data that maintain high accuracy while forecasting values is highly acceptable. Due to the lack of prediction accuracy with the existing well-established model, a new correlation is proposed by multiple regression analyses considering the temperature and concentrations as the variables as expressed in **Eq.32**.

$$\frac{k_{nf}}{k_{bf}} = 0.9804 + 1.799\varphi + 0.0018\,T \tag{32}$$

This correlation has an accuracy level of R^2= 0.987 with a standard error of 0.009, ensuring a highly reliable prediction of k for the hybrid Ionanofluid IL+DEG/Al_2O_3+CuO. To assess the accuracy of this model, **Figure 13**c is plotted that shows the predicted values vs experimental values with the 2% deviation line. The following formula assessed the deviations between the experimental and predicted values:

$$\text{Deviation Margin} = \left[\frac{\left(\frac{k_{nf}}{k_{bf}}\right)_{Exp} - \left(\frac{k_{nf}}{k_{bf}}\right)_{Pred}}{\left(\frac{k_{nf}}{k_{bf}}\right)_{Pred}}\right] \times 100\% \tag{33}$$

It is obvious from **Figure 13**c that the deviation for all predicted data is below 2% and almost lies on the equality line, which indicates an excellent agreement of predicted data with experimental data.

(a) (b)

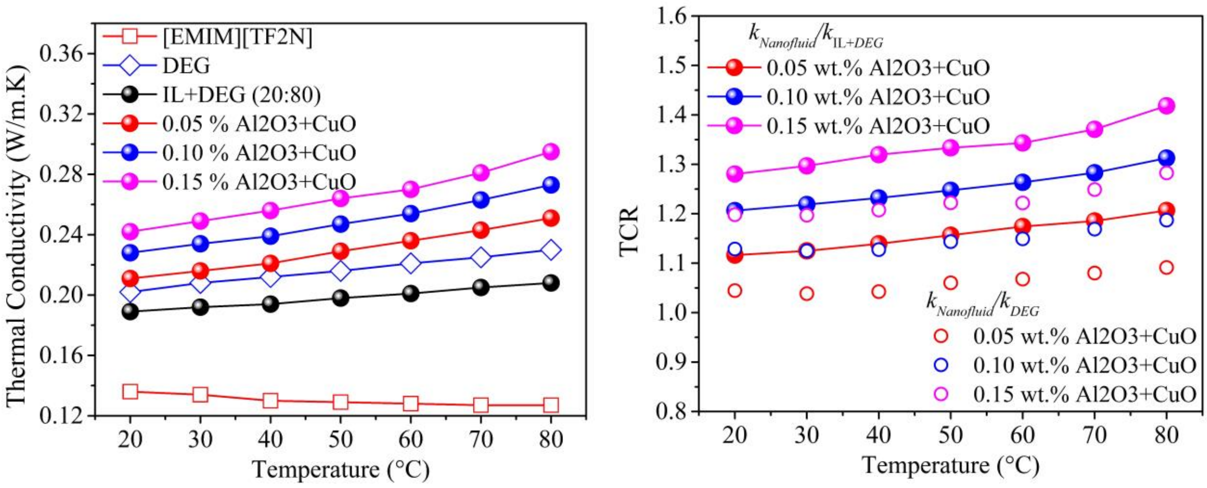

(c)

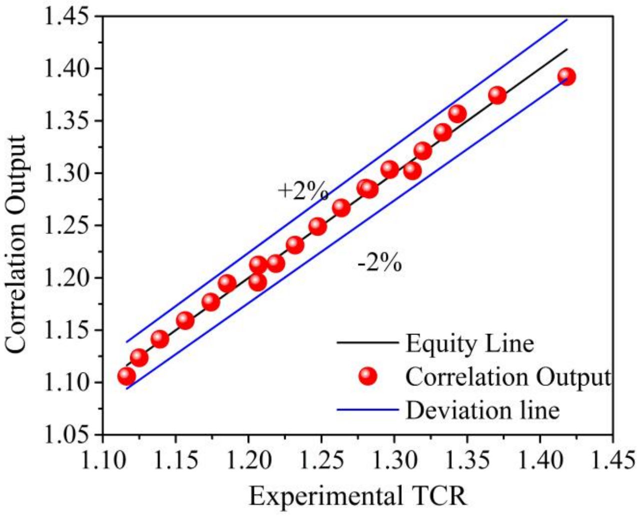

Figure 13. (a) Experimental TC vs. temperature (b) TCR vs. temperature of the base fluid and Ionanofluid at different concentrations of Al_2O_3+CuO, (c) correlation output vs. experimental TCR values with 2% deviation lines.

3.6. Rheological properties

Figure 14a depicts the dynamic viscosity, μ of IL+DEG and hybrid [EMIM][Tf_2N]+DEG/Al_2O_3+CuO Ionanofluids as a function of temperature, while **Figure 14**b demonstrates the μ ratio vs. temperature. The μ of the binary [EMIM][Tf2N]+DEG fluid, as shown in the figure, varies from 22.8 to 9.6 mPa.s in the temperature range of 20–55 °C, which is lower than that of pure [EMIM][Tf_2N] (Fröba et al., 2008) and higher than that of pure DEG (Li et al., 2014), and follows the Arrhenius expression (**Eq.34**).The addition of 0.05 wt.% Al_2O_3+CuO, on the other hand, raises the from 29.63 to 32.92 mPa.s at 20 °C. The increases further as the nanoparticle loading increases, reaching 38.8 mPa.s when the concentration is increased to 0.15 wt.% at the same temperature. At 20 °C, concentrations of 0.15 wt.% cause a maximum 31 % increase in the μ, and the ratio remains nearly constant throughout the temperature range studied. The increasing phenomenon of the μ with increasing nanoparticles loading is consistent with most previous studies (Li et al., 2016; Mostafizur et al., 2014) and can be explained by the fact that the inclusion of nanoparticles increases shear stress, weakening the particle's adhesion force. Furthermore, the temperature-dependent viscosity curve shows a sharp decrease in the μ with increasing temperature due to the particles' increased Brownian motion and the fluid molecules' increased mobility at higher temperatures. Nevertheless, the Newtonian behavior of the formulated Ionanofluid is evidenced by the independence of the with shear rate (**Figure 14**c). Higher μ of the working fluid significantly reduces the hydrothermal efficiency of the thermal system, resulting from a higher pressure drop penalty. Thus, the primary goal of developing nanofluids is to increase thermal conductivity while keeping the μ as low as possible. The highest penalty in the μ is 31%, which is lower than the maximum TC enhancement of 41.8 %. As a result, formulated Ionanofluid can be expected to improve the overall hydrothermal performance.

$$log\,\mu_{IL+DEG} = X_{IL} log\mu_{IL} + X_{DEG} log\mu_{DEg} \tag{34}$$

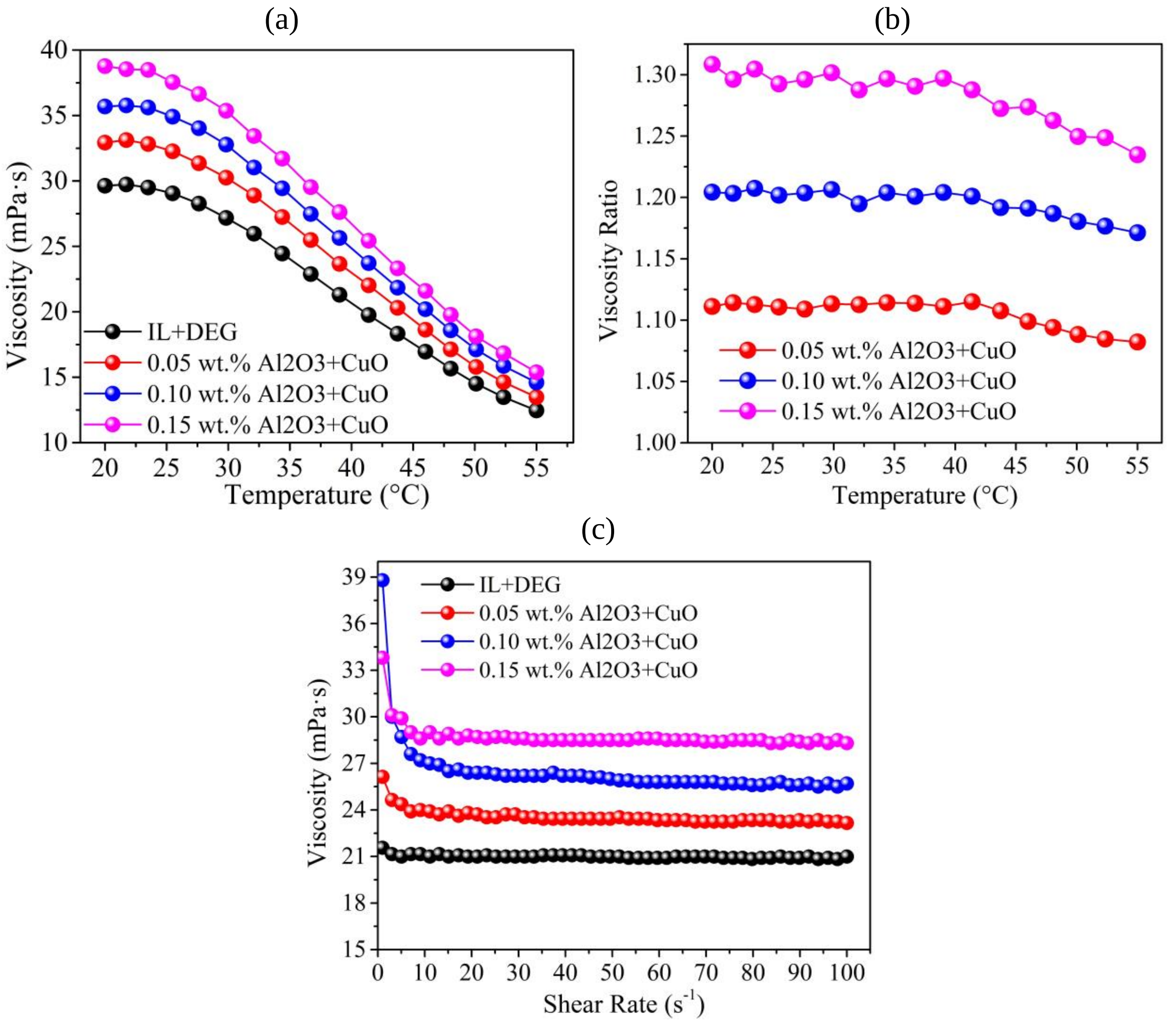

Figure 14. (a) Experimental viscosity vs. temperature (b) viscosity ratio vs. temperature, (c) viscosity vs. shear rate of the base fluid and Ionanofluid at different concentrations of Al_2O_3+CuO.

3.7. Density

The experimental density, ρ of IL, DEG, IL+DEG, and ionanofluids at varying concentrations are plotted in **Figure 15** as a function of temperature. The measurement uncertainty was less than 5% for each sample. The ρ of [EMIM][Tf_2N] linearly decrease from 1.534 gm/cm^3 to 1.484 gm/cm^3 as the temperature increases from 10 °C to 60 °C showing strong consistency with the measured data by (Součková et al., 2014). On the other hand, the DEG exhibits comparatively low densities ranging from 1.121 gm/cm^3 to 1.079 gm/cm^3 for the same temperature fluctuations. The mixture of IL+DEG shows an intermediate density range starting from 1.204 gm/cm^3 at 10 °C and linearly decreased to 1.159 gm/cm^{3}as the temperature reaches 60 °C. The dispersed nanoparticles further increase the density of the ionanofluids due to the addition of solid particles that increase the total mass of the ionanofluids more significantly than the volume of the ionanofluids. Nevertheless, the density of the ionanofluids can be predicted precisely with the approximation using **Eq.35** of the mixing rule.

$$\rho_{inf} = \rho_{np}\varphi_{np} + (1 - \varphi_{np})\rho_{IL+DEG} \tag{35}$$

However, with the increasing temperature, the density of Ionanofluids experiences a linear decrement due to the expanded volume at a higher temperature. Since density is an important parameter in heat transfer engineering and energy storage systems, the knowledge of density measurement with temperature and particle concentration plays an important role in determining system efficiency. For instance, sensible heat is a function of fluid density and heat capacity, a key parameter in the energy storage system.

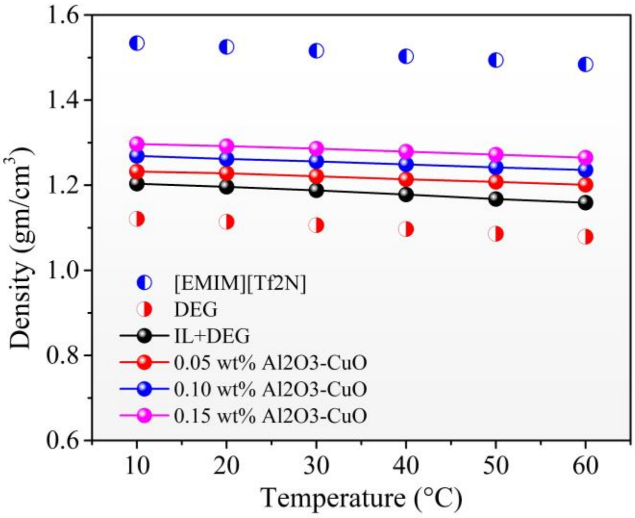

Figure 15. The experimental density of IL, DEG, LL+DEG, and ionanofluids at different concentrations with error bar.

3.8. Thermogravimetric Analyses

Figure 16 depicts a plot of % weight vs. temperature demonstrated by TGA analyses to assess thermal stability at elevated temperatures. The curve shows that the binary mixture of IL and DGA undergoes a two-step decomposition while the sample is heated. Because 95 % mass remained unchanged, the binary mixture was thermally stable up to 150 °C. Above 150 °C, however, the first decomposition occurs, which corresponds to the disintegration of DEG, and it is wholly decomposed at nearly 250 °C. The remaining 25% of the sample was IL, which was thermally stable up to 450 °. The IL began to disintegrate in the second step decomposition at 450 °C and reached complete decomposition at nearly 500 °C.

Nonetheless, the two-step decomposition and acceptable percent weight at the decomposition zone confirm that the binary solution's constituents were uniformly mixed. The thermal behavior of both components was not affected by the mixture. On the other hand, addition of nanoparticles had a negligible shift when compared to the base IL+DEG decomposition line, indicating that dispersed nanoparticles at very low loadings do not change decomposition behavior. As a result, these IL+DEG-based Ionanofluids can be used for solar energy storage at temperatures up to 150 °C.

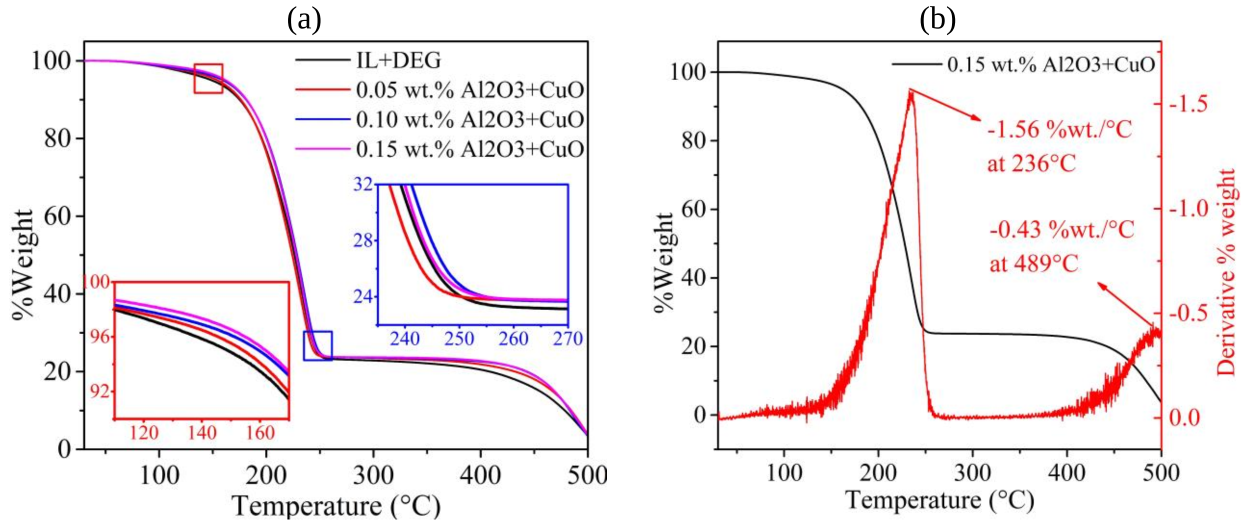

Figure 16. TGA curve of Pure IL+DEG binary solution and its Ionanofluids at different concentrations of Al_2O_3 + CuO nanoparticles.

3.9. Uncertainties of thermophysical measurements

The accuracy of measurements is critical for experimental studies on the thermophysical characteristics of formulated Ionanofluid to ensure precise results interpretation. In order to present a quantitative description of how reliable experimental results are, an uncertainty analysis is required. Direct measurements of thermal conductivity and density have unavoidable uncertainties. A simple approach is used to determine the uncertainty. It is possible to compute the mean relative uncertainty of the complex quantity by using the general relation (Coleman & Steele, 2018): Tables S1 and S2 (Supplemental material) presents the experimental values for thermal conductivities and densities, along with the measurement uncertainties. **Table S1** and **Table S2** (Supplementary material) represents the experimental data of the thermal conductivities and densities and their associated measurement uncertainties. Viscosity measurements need specialized equipment. Thus, uncertainties emerge from instrument precision. Professional temperature sensors with defined accuracies were used to measure temperatures. **Table S2** shows the experimental viscosities and measurement uncertainties.

3.10. Validation

The results of the solar cell temperature at an irradiation intensity of 1000 W/m^2 and several flow rates (0.5 to 3 LPM) were obtained from the present numerical model, validated with (Nasrin, Hasanuzzaman, et al., 2018a). **Table 7**, expresses this validation and provides a very good accord with the numerical findings (Nasrin, Hasanuzzaman, et al., 2018a) and the experimental findings of (Rahman et al., 2017). The electrical and thermal efficiencies are validated with (Nasrin, Rahim, et al., 2018) (**Table 8**), in which they used MWCNT/water nanofluid and perform simulation at 0.1% concentration and 1000 W/m^2 irradiance level. The design of heat exchanger used by (Nasrin, Rahim, et al., 2018) is quad helical tubing. Our results are quite promising with this paper however a little discrepancy is due to the different design and different nanofluid used.

Table 7. Validation of average cell Temperature.

Flowrate (LPM)	**Cell Temperature (°C)**		
	Present Research	**Numerical Study (Nasrin, Hasanuzzaman, et al., 2018a)**	**Experimental Study (Rahman et al., 2017).**
0.5	52.56	51.11	52.88
1	49.85	48.04	50.23
3	47.10	45.76	47.73

Table 8. Validation of Electrical and thermal efficiency.

Nanoparticle Concentration (Wt.%)	**Electrical Efficiency (%)**		**Thermal Efficiency (%)**	
	Present Research	**(Nasrin, Rahim, et al., 2018)**	**Present Research**	**(Nasrin, Rahim, et al., 2018)**
0.1%	11.50	11.96	62	73.5

3.11. Performance of Ionanofluid assisted PV/T collector

Figure 17 represent the pressure drop variation with flow rate. It is obvious from the **Figure 17** that pressure drop increases with flow rate for each nanofluid. An increase in flow rate at a constant concentration level leads to an increase in nanofluid velocity, which, according to the well-known Darcy–Weisbach relation (Brater & King, 1996), leads to an increase in the pressure drop. The pressure drop also rises as the concentration of nanoparticles in the base fluid increases, attributable to an increase in viscosity as the concentration of nanoparticles in the base fluid rises. When compared to the base fluid, the introduction of the nanoparticle at 0.05 % enhanced the pressure drop by 24 %. The viscosity of the Ionanofluid rose as the concentration of nanoparticles increased, and the maximum pressure drop at a flow rate of 0.5 LPM was reported to be 72 %. In addition to this, it can be noticed that the pressure drop consistently becomes larger with the rise in flow rate. As a result, at the maximum flowrate of 4LPM, the base fluid and nanofluid suffer the greatest penalty in pressure drop at all concentrations. However, when comparing 0.15 % Al_2O_3+CuO Ionanofluid to pure IL+DEG, the current simulations show a maximum increase of roughly 82 %. The present simulations' findings in the provided range of flow rate and nanoparticle concentrations are compatible with the results of (El-Maghlany et al., 2016; Safaei et al., 2016).

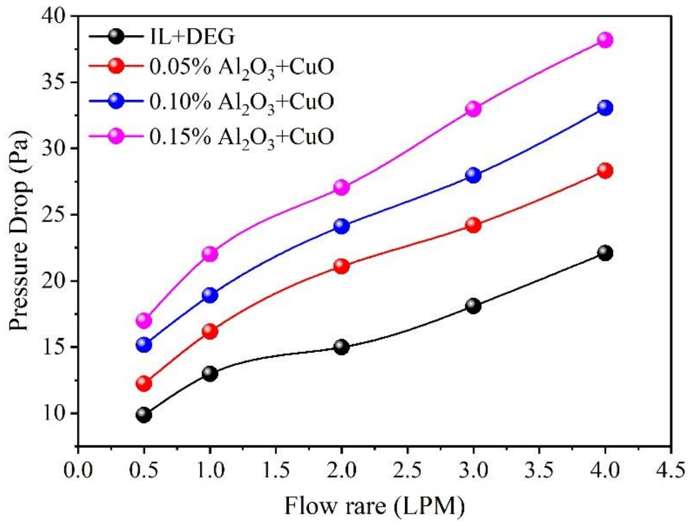

Figure 17. Pressure drop for different nanofluids with flowrate.

To maintain the PV module temperature in the permissible limit, different coolants were used in this study. **Figure 18**a depicts the relationship between the average temperature of the PV cell and the flow rate. All nanofluids showed a decline with significant variation due to the increased convection rate from the module, which lowers the average cell temperature as flow rate increases. At a maximum flow rate of 4LPM, the temperature of the PV surface due to IL+DEG, 0.05%, 0.1%, and 0.15% are 65°C, 54°C, 48°C, and 39.5°C, respectively. Comparing with the previous works, IL+DEG/(Al2O3+CuO) Ionanofluid, at 0.15 wt. %, outperforms Mxene/Palm oil(Samylingam et al., 2020) and MXene/ Soyabean oil (Rubbi et al., 2020) based nanofluids, where the panel temperature was 42°C and 40°C, respectively, which is somewhat higher than 39.5°C obtained from current study. **Figure 18**b depicts the heat transfer coefficient and the flow rate relationship. It can be seen from the plot that the heat transfer coefficient increases in proportion to the flow rate, regardless of the fluid used in the current study. Compared to the IL+DEG based PVT system, a maximum percentage enhancement of 38.77 % is achieved at 4LPM for 0.15% (Al_2O_3+CuO).

Thermal efficiency variation with flow rate is depicted in **Figure 18**c for all nanofluids. Regardless of the type of coolant, the higher the flow rates, the better the thermal efficiency of the PVT system. At a maximum flow rate of 4LPM, IL+DEG has a thermal efficiency of 56%, 0.05 % (Al_2O_3+CuO) has a thermal efficiency of 58%, 0.10 % (Al_2O_3+CuO) has a thermal efficiency of 63%, and 0.15 % (Al_2O_3+CuO) has a thermal efficiency of 69%. The results indicate that 0.15 % (Al_2O_3+CuO) nanofluid performs better than the other three nanofluids and high heat transfer capacity. Compared to the IL+DEG-based PVT system, 0.15 % (Al_2O_3+CuO) increased thermal efficiency by 23.21 %. **Figure 18**d shows the comparison between IL+DEG, 0.05% (Al_2O_3+CuO), 0.1% (Al_2O_3+CuO), and 0.15% (Al_2O_3+CuO) nanofluid to notice the effect on PV module electrical efficiency at an irradiance level of 1000W/m^2 and varying flow rates. The electrical efficiency increases with the flow rate. For 0.05% (Al_2O_3+CuO) it increases from 9.8% to 11.1%, for 0.1% (Al_2O_3+CuO) it increases from 10.4% to 12.1%, and for 0.15% (Al_2O_3+CuO) it increases from 10.8% to 12.7% in the flow rate range from 0.05 to 4LPM. Hence, by using 0.05% (Al_2O_3+CuO) nanofluid in the hybrid PVT system, a 13.26% electrical efficiency improvement is achieved compared to the IL+DEG-based PVT system at a flow rate of 4LPM. Furthermore, using 0.15% (Al_2O_3+CuO), an electrical efficiency improvement of 29.59% is achieved compared to IL+DEG as a coolant at a flow rate of 4LPM.

(a) (b)

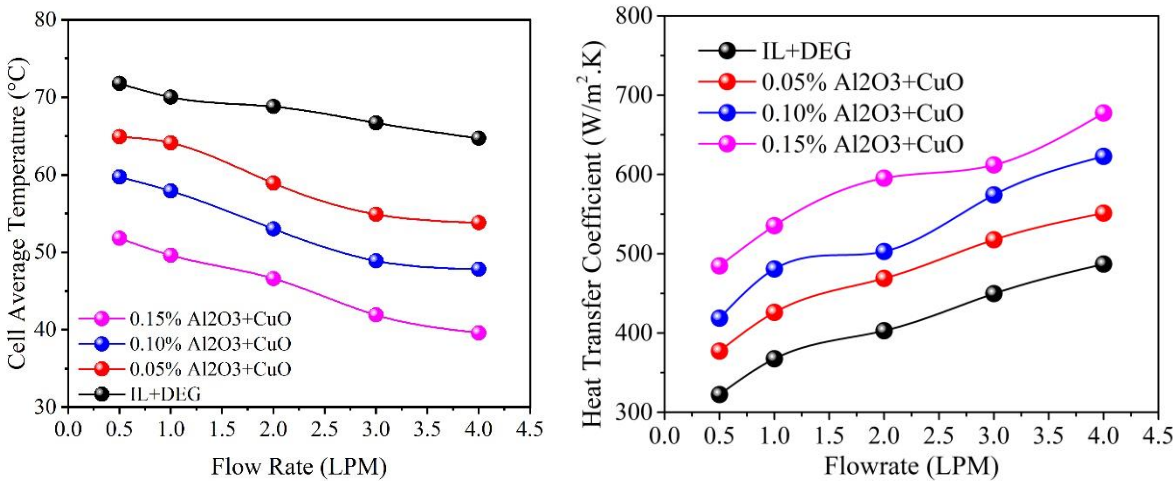

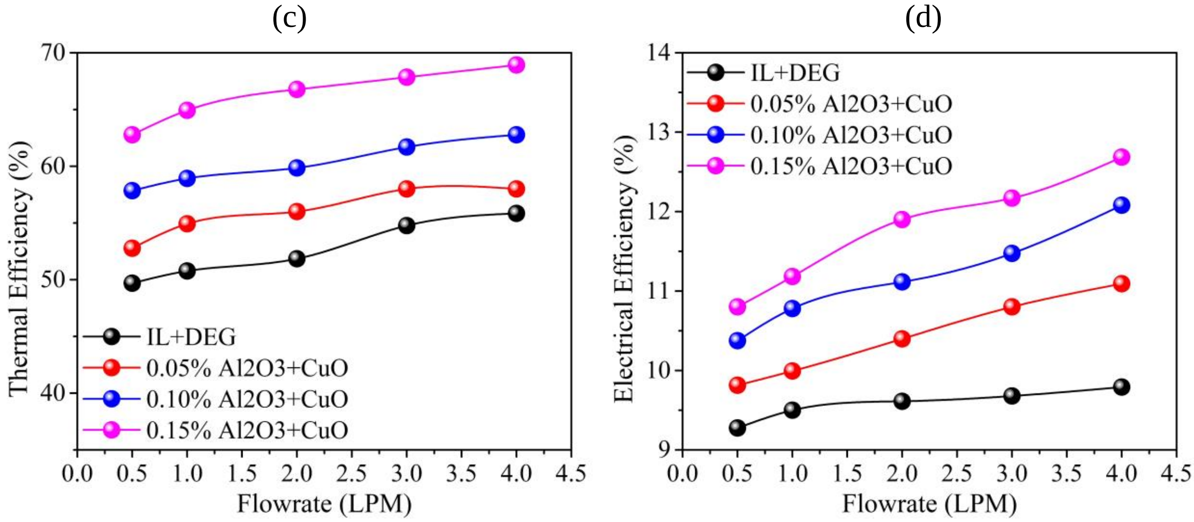

Figure 18. (a) PV Cell average temperature as a function of flow rate using different types of coolant, (b) PV/T system heat transfer coefficient variation with mass flow rate using different types of coolant. All at an irradiance level of 1000 W/m^2, (c) Thermal efficiency of PV/T system as a function of flow rate with different types of coolant, d) Electrical efficiency of PV/T system as a function of flow rate with different types of coolant.

Figure 19(a) represents the trends of electrical efficiency obtained with time for all working fluid at 4LPM. Average PV panel efficiency obtained was 11.1%, 11.7%, and 12.7% for conventional PV, IL+DEG, and Al_2O_3-CuO/IL+DEG respectively. Use of hybrid nanofluid led to increase the electrical efficiency of PVT system in comparison to base fluid. Enhancement in electrical efficiency for Al_2O_3-CuO/IL+DEG was more than both the base fluid and conventional PV because of higher thermal conductivity of Al_2O_3-CuO nanoparticles which allows more heat removal from system in less time than IL+DEG. As clear from **Figure 19**(b), thermal efficiency of PV/T system at 4LPM was determined to be 56%, and 69% for IL+DEG, and Al_2O_3-CuO/IL+DEG respectively. Thermal efficiency of PV/T system was enhanced by increasing flow rate because at higher flow rates temperature difference between inlet and outlet of PV/T system was enhanced due to high heat absorption of nanofluid from system. **Table 9** presents a comparison of the electrical and thermal performance of these Ionanofluid, water, and water/MWCNT. The data clearly shows that IL+DEG outperforms water and falls short of water-based nanofluids in terms of thermal efficiency, owing to water's greater thermal conductivity than IL+DEG. Nonetheless, Ionanofluid was reportedly more efficient than water/MWCNT nanofluid in terms of electrical efficiency. The results of this research indicate that the formulated Ionanofluid may be a viable option as a substitute for water liquid in medium temperature range PV/T systems where water-based nanofluid is not practicable owing to thermal degradation concerns.

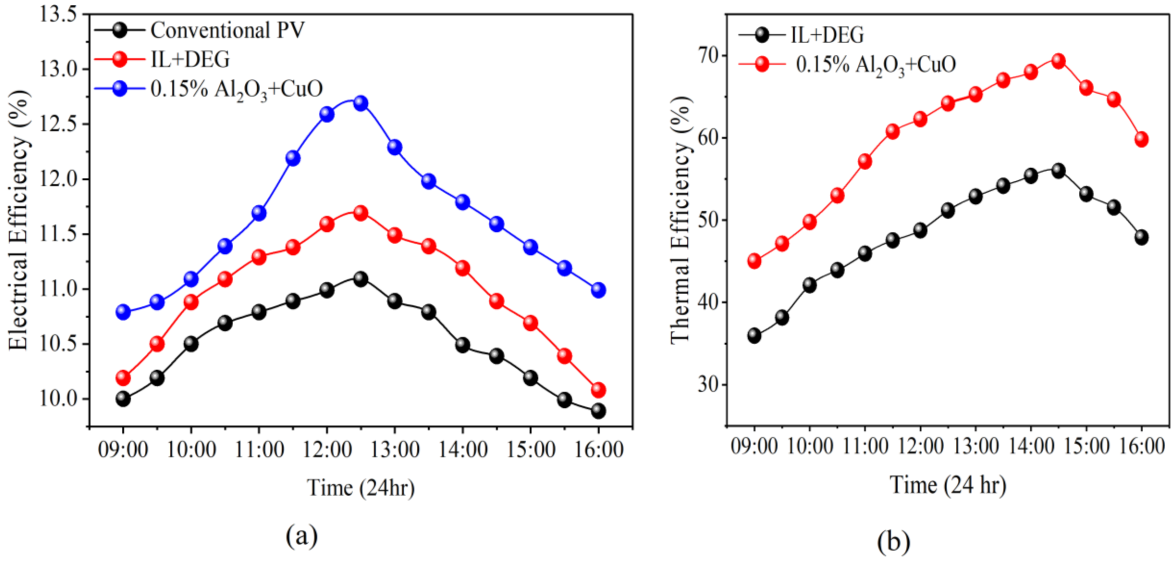

Figure 19. (a) Electrical and (b) Thermal efficiency with time for a typical day at a flowrate of 4LPM

Table 9. Comparison of Electrical and thermal efficiency between Ionanofluid, water and water/MWCNT nanofluids.

Coolants	Electrical Efficiency	Thermal Efficiency	References
Al_2O_3-CuO/IL+DEG	12.7%	69%	This Work
Water/MWCNT	12.5%	79%	(Fayaz et al., 2018)
Water	14.58	58.77%	(Menon et al., 2022)

4. Conclusion:

In this study, a new class of surfactant-free hybrid Ionanofluid ([EMIM][Tf_2N] +DEG/Al_2O_3+CuO) synthesized at three different concentrations of 0.05, 0.10, and 0.15 wt. % for medium temperature range coolant application. The Zeta potential study, which demonstrated excellent dispersion stability despite the absence of any additional stabilizing agents, provided conclusive evidence that the incorporation of Ionic Liquid served as a stability promoting agents in addition to a working fluid. The chemical and thermal stability assessments confirmed that the formulated Ionanofluid was free of any chemical reaction and that no significant thermal degradation occurred until 200 °C. The experimental thermophysical measurement and numerical performance assessment of a PV/T panel showed significant improvements. Ionanofluids significantly improved the thermal and electrical performance of the PVT system. The key findings of this study are summarized below.

- In comparison to IL+DEG, the maximum increase in thermal conductivity was achieved at concentrations of 0.15 wt.% of about 41.8% increase. At the same concentration, the viscosity was affected by a penalty of 31%. Despite this, the synthesized Ionanofluid behaved as a Newtonian fluid, as evidenced by the presence of a constant viscosity line across a range of shear rates.

- The incorporation of Ionanofluids as the coolants in a PV/T panel showed a maximum of 69% thermal efficiency at 0.15 wt.% concentrations of Al_2O_3+CuO higher than 63% (0.10 wt.% Al_2O_3+CuO), 58% (0.05 wt.% Al_2O_3+CuO), and 56% (pure IL+DEG). The temperature of the PVT panel was maximally dropped from 65 °C to 40 °C when IL+DEG was replaced with IL+DEG/Al_2O_3+CuO (0.15 wt.%). An electrical efficiency of nearly 12.7% was observed with 0.15 % Al2O3+CuO as a coolant at a flow rate of 4LPM, which resulted in an improvement of 29.91 % over IL+DEG at the same flow rate.

- The formulated Ionanofluid performed thermally more efficiently than water, but less efficiently than water-based nanofluids like MWCNT/Water nanofluid. In contrast, the Ionanofluid performed better than MWCNT/Water nanofluid in terms of electrical efficiency. To conclude, the formulated Ionanofluid can be a viable alternative to water-based nanofluids for medium-temperature-based coolant applications where water-based nanofluids are not feasible. In addition, the exergetic performance of using Ionanofluid in a solar PV/T system can be demonstrated through further research.

Acknowledgement:

This research was funded by Universiti Malaysia Pahang, grant No. RDU213308 and RDU192209.

References:

Abdallah, S. R., Elsemary, I. M. M., Altohamy, A. A., Abdelrahman, M. A., Attia, A. A. A., & Abdellatif, O. E. (2018). Experimental investigation on the effect of using nano fluid (Al2O3-Water) on the performance of PV/T system. *Thermal Science and Engineering Progress*, *7*, 1-7. https://doi.org/https://doi.org/10.1016/j.tsep.2018.04.016

Abdollahi, S., Mortaheb, H. R., Ghadimi, A., & Esmaeili, M. (2018). Improvement in separation performance of Matrimid®5218 with encapsulated [Emim][Tf2N] in a heterogeneous structure: CO2/CH4 separation. *Journal of Membrane Science*, *557*, 38-48. https://doi.org/https://doi.org/10.1016/j.memsci.2018.04.026

Agafonov, A. V., Grishina, E. P., Kudryakova, N. O., Ramenskaya, L. M., Kraev, A. S., & Shibaeva, V. D. (2022). Ionogels: Squeeze flow rheology and ionic conductivity of quasi-solidified nanostructured hybrid materials containing ionic liquids immobilized on halloysite. *Arabian Journal of Chemistry*, *15*(1), 103470. https://doi.org/https://doi.org/10.1016/j.arabjc.2021.103470

Al-Waeli, A. H. A., Chaichan, M. T., Kazem, H. A., & Sopian, K. (2019). Evaluation and analysis of nanofluid and surfactant impact on photovoltaic-thermal systems. *Case Studies in Thermal Engineering*, *13*, 100392. https://doi.org/https://doi.org/10.1016/j.csite.2019.100392

Alkathiri, A. A., Jamshed, W., Uma Devi S, S., Eid, M. R., & Bouazizi, M. L. (2022). Galerkin finite element inspection of thermal distribution of renewable solar energy in presence of binary nanofluid in parabolic trough solar collector. *Alexandria Engineering Journal*, *61*(12), 11063-11076. https://doi.org/https://doi.org/10.1016/j.aej.2022.04.036

Alous, S., Kayfeci, M., & Uysal, A. (2019). Experimental investigations of using MWCNTs and graphene nanoplatelets water-based nanofluids as coolants in PVT systems. *Applied Thermal Engineering*, *162*, 114265. https://doi.org/https://doi.org/10.1016/j.applthermaleng.2019.114265

Arif, M. S. B., Avob, S. M., Yahya, S. M., Mustafa, U., Ado, M., & Khan, Z. A. (2018, 7-10 Oct. 2018). Effect of Zn-H20 Nanofluid Back-Flow Channels on the Efficiency and Electrical Power Output of a Solar PV Panel Used in Standalone PV System. 2018 IEEE PES Asia-Pacific Power and Energy Engineering Conference (APPEEC),

Bakthavatchalam, B., Habib, K., Saidur, R., Saha, B. B., & Irshad, K. (2020). Comprehensive study on nanofluid and ionanofluid for heat transfer enhancement: A review on current and future perspective. *Journal of Molecular Liquids*, *305*, 112787.

Bonnot, K., Doblas, D., Schnell, F., Schlur, L., & Spitzer, D. (2015). Chip Calorimetry for the Sensitive Identification of Hexogen and Pentrite from Their Decomposition inside Copper Oxide Nanoparticles. *Analytical Chemistry*, *87*(18), 9494-9499. https://doi.org/10.1021/acs.analchem.5b02773

Brater, E. F., & King, H. W. (1996). Handbook of hydraulics: For the solution of hydraulic engineering problems.

Bretado-de los Rios, M. S., Rivera-Solorio, C. I., & Nigam, K. D. P. (2021). An overview of sustainability of heat exchangers and solar thermal applications with nanofluids: A review. *Renewable and Sustainable Energy Reviews*, *142*, 110855. https://doi.org/https://doi.org/10.1016/j.rser.2021.110855

Chakraborty, S., & Panigrahi, P. K. (2020). Stability of nanofluid: A review. *Applied Thermal Engineering*, *174*, 115259. https://doi.org/https://doi.org/10.1016/j.applthermaleng.2020.115259

Chaurasia, S. R., & Sarviya, R. M. (2020). Thermal performance analysis of CuO/water nanofluid flow in a pipe with single and double strip helical screw tape. *Applied*

Thermal Engineering, *166*, 114631. https://doi.org/https://doi.org/10.1016/j.applthermaleng.2019.114631

Coleman, H. W., & Steele, W. G. (2018). *Experimentation, validation, and uncertainty analysis for engineers*. John Wiley & Sons.

El-Maghlany, W. M., Hanafy, A. A., Hassan, A. A., & El-Magid, M. A. (2016). Experimental study of Cu–water nanofluid heat transfer and pressure drop in a horizontal double-tube heat exchanger. *Experimental Thermal and Fluid Science*, *78*, 100-111. https://doi.org/https://doi.org/10.1016/j.expthermflusci.2016.05.015

Elmir, M., Mehdaoui, R., & Mojtabi, A. (2012). Numerical Simulation of Cooling a Solar Cell by Forced Convection in the Presence of a Nanofluid. *Energy Procedia*, *18*, 594-603. https://doi.org/https://doi.org/10.1016/j.egypro.2012.05.072

Fayaz, H., Nasrin, R., Rahim, N. A., & Hasanuzzaman, M. (2018). Energy and exergy analysis of the PVT system: Effect of nanofluid flow rate. *Solar Energy*, *169*, 217-230. https://doi.org/https://doi.org/10.1016/j.solener.2018.05.004

Fayaz, H., Rahim, N. A., Hasanuzzaman, M., Nasrin, R., & Rivai, A. (2019). Numerical and experimental investigation of the effect of operating conditions on performance of PVT and PVT-PCM. *Renewable Energy*, *143*, 827-841. https://doi.org/https://doi.org/10.1016/j.renene.2019.05.041

Fayaz, H., Rahim, N. A., Hasanuzzaman, M., Rivai, A., & Nasrin, R. (2019). Numerical and outdoor real time experimental investigation of performance of PCM based PVT system. *Solar Energy*, *179*, 135-150. https://doi.org/https://doi.org/10.1016/j.solener.2018.12.057

Fröba, A. P., Kremer, H., & Leipertz, A. (2008). Density, Refractive Index, Interfacial Tension, and Viscosity of Ionic Liquids [EMIM][EtSO4], [EMIM][NTf2], [EMIM][N(CN)2], and [OMA][NTf2] in Dependence on Temperature at Atmospheric Pressure. *The Journal of Physical Chemistry B*, *112*(39), 12420-12430. https://doi.org/10.1021/jp804319a

Ge, R., Hardacre, C., Nancarrow, P., & Rooney, D. W. (2007). Thermal Conductivities of Ionic Liquids over the Temperature Range from 293 K to 353 K. *Journal of Chemical & Engineering Data*, *52*(5), 1819-1823. https://doi.org/10.1021/je700176d

Hasan, H. A., Sopian, K., Jaaz, A. H., & Al-Shamani, A. N. (2017). Experimental investigation of jet array nanofluids impingement in photovoltaic/thermal collector. *Solar Energy*, *144*, 321-334. https://doi.org/https://doi.org/10.1016/j.solener.2017.01.036

Hendricks, J. H. C., & van Sark, W. G. J. H. M. (2013). Annual performance enhancement of building integrated photovoltaic modules by applying phase change materials [https://doi.org/10.1002/pip.1240]. *Progress in Photovoltaics: Research and Applications*, *21*(4), 620-630. https://doi.org/https://doi.org/10.1002/pip.1240

Hormozi Moghaddam, M., & Karami, M. (2022). Heat transfer and pressure drop through mono and hybrid nanofluid-based photovoltaic-thermal systems [https://doi.org/10.1002/ese3.1073]. *Energy Science & Engineering*, *n/a*(n/a). https://doi.org/https://doi.org/10.1002/ese3.1073

Hu, G., Ning, X., Hussain, M., Sajjad, U., Sultan, M., Ali, H. M., Shah, T. R., & Ahmad, H. (2021). Potential evaluation of hybrid nanofluids for solar thermal energy harvesting: A review of recent advances. *Sustainable Energy Technologies and Assessments*, *48*, 101651. https://doi.org/https://doi.org/10.1016/j.seta.2021.101651

Hunter, R. J. (2013). *Zeta potential in colloid science: principles and applications* (Vol. 2). Academic press.

Kumar, V., & Sahoo, R. R. (2019). Viscosity and thermal conductivity comparative study for hybrid nanofluid in binary base fluids. *Heat Transfer—Asian Research*, *48*(7), 3144-3161. https://doi.org/10.1002/htj.21535

Li, L., Zhang, J., Li, Q., Guo, B., Zhao, T., & Sha, F. (2014). Density, viscosity, surface tension, and spectroscopic properties for binary system of 1,2-ethanediamine+diethylene glycol. *Thermochimica Acta*, *590*, 91-99. https://doi.org/https://doi.org/10.1016/j.tca.2014.05.034

Li, X., Zou, C., & Qi, A. (2016). Experimental study on the thermo-physical properties of car engine coolant (water/ethylene glycol mixture type) based SiC nanofluids. *International Communications in Heat and Mass Transfer*, *77*, 159-164. https://doi.org/https://doi.org/10.1016/j.icheatmasstransfer.2016.08.009

Liu, J., Wang, F., Zhang, L., Fang, X., & Zhang, Z. (2014). Thermodynamic properties and thermal stability of ionic liquid-based nanofluids containing graphene as advanced heat transfer fluids for medium-to-high-temperature applications. *Renewable Energy*, *63*, 519-523. https://doi.org/https://doi.org/10.1016/j.renene.2013.10.002

Main, K. L., Eberl, B. K., McDaniel, D., Tikadar, A., Paul, T. C., & Khan, J. A. (2021). Nanoparticles size effect on thermophysical properties of ionic liquids based nanofluids. *Journal of Molecular Liquids*, *343*, 117609. https://doi.org/https://doi.org/10.1016/j.molliq.2021.117609

Mei, J., Shao, Y., Lu, S., Ma, Y., & Ren, L. (2018). Synthesis of Al2O3 with tunable pore size for efficient formaldehyde oxidation degradation performance. *Journal of Materials Science*, *53*(5), 3375-3387. https://doi.org/10.1007/s10853-017-1795-x

Menon, G. S., Murali, S., Elias, J., Aniesrani Delfiya, D. S., Alfiya, P. V., & Samuel, M. P. (2022). Experimental investigations on unglazed photovoltaic-thermal (PVT) system using water and nanofluid cooling medium. *Renewable Energy*, *188*, 986-996. https://doi.org/https://doi.org/10.1016/j.renene.2022.02.080

Minea, A.-A., & El-Maghlany, W. M. (2017). Natural convection heat transfer utilizing ionic nanofluids with temperature-dependent thermophysical properties. *Chemical Engineering Science*, *174*, 13-24. https://doi.org/https://doi.org/10.1016/j.ces.2017.08.028

Minea, A. A., & Murshed, S. M. S. (2018). A review on development of ionic liquid based nanofluids and their heat transfer behavior. *Renewable and Sustainable Energy Reviews*, *91*, 584-599. https://doi.org/https://doi.org/10.1016/j.rser.2018.04.021

Mohammad, S. T., Al-Kayiem, H. H., Aurybi, M. A., & Khlief, A. K. (2020). Measurement of global and direct normal solar energy radiation in Seri Iskandar and comparison with other cities of Malaysia. *Case Studies in Thermal Engineering*, *18*, 100591. https://doi.org/https://doi.org/10.1016/j.csite.2020.100591

Mostafizur, R. M., Abdul Aziz, A. R., Saidur, R., Bhuiyan, M. H. U., & Mahbubul, I. M. (2014). Effect of temperature and volume fraction on rheology of methanol based nanofluids. *International Journal of Heat and Mass Transfer*, *77*, 765-769. https://doi.org/https://doi.org/10.1016/j.ijheatmasstransfer.2014.05.055

Motamedi, M., Chung, C.-Y., Rafeie, M., Hjerrild, N., Jiang, F., Qu, H., & A. Taylor, R. (2019). Experimental Testing of Hydrophobic Microchannels, with and without Nanofluids, for Solar PV/T Collectors. *Energies*, *12*(15), 3036. https://www.mdpi.com/1996-1073/12/15/3036

Naghdbishi, A., Yazdi, M. E., & Akbari, G. (2020). Experimental investigation of the effect of multi-wall carbon nanotube – Water/glycol based nanofluids on a PVT system integrated with PCM-covered collector. *Applied Thermal Engineering*, *178*, 115556. https://doi.org/https://doi.org/10.1016/j.applthermaleng.2020.115556

Nahar, A., Hasanuzzaman, M., & Rahim, N. A. (2017). Numerical and experimental investigation on the performance of a photovoltaic thermal collector with parallel plate flow channel under different operating conditions in Malaysia. *Solar Energy*, *144*, 517-528. https://doi.org/https://doi.org/10.1016/j.solener.2017.01.041

Nasrin, R., Hasanuzzaman, M., & Rahim, N. A. (2018a). Effect of high irradiation and cooling on power, energy and performance of a PVT system. *Renewable Energy*, *116*, 552-569. https://doi.org/https://doi.org/10.1016/j.renene.2017.10.004

Nasrin, R., Hasanuzzaman, M., & Rahim, N. A. (2018b). Effect of high irradiation on photovoltaic power and energy [https://doi.org/10.1002/er.3907]. *International Journal of Energy Research*, *42*(3), 1115-1131. https://doi.org/https://doi.org/10.1002/er.3907

Nasrin, R., & Parvin, S. (2012). Investigation of buoyancy-driven flow and heat transfer in a trapezoidal cavity filled with water–Cu nanofluid. *International Communications in Heat and Mass Transfer*, *39*(2), 270-274. https://doi.org/https://doi.org/10.1016/j.icheatmasstransfer.2011.11.004

Nasrin, R., Rahim, N. A., Fayaz, H., & Hasanuzzaman, M. (2018). Water/MWCNT nanofluid based cooling system of PVT: Experimental and numerical research. *Renewable Energy*, *121*, 286-300. https://doi.org/https://doi.org/10.1016/j.renene.2018.01.014

Nasrin, R. N., & Hossain, M. S. (2021). Numerical analysis of photovoltaic power generation in different locations of Bangladesh. *Journal of Computational & Applied Research in Mechanical Engineering (JCARME)*, *10*(2), 373-389. https://doi.org/10.22061/jcarme.2019.4601.1558

Rahman, M. M., Hasanuzzaman, M., & Rahim, N. A. (2017). Effects of operational conditions on the energy efficiency of photovoltaic modules operating in Malaysia. *Journal of Cleaner Production*, *143*, 912-924. https://doi.org/https://doi.org/10.1016/j.jclepro.2016.12.029

Rajabpour, A., Seif, R., Arabha, S., Heyhat, M. M., Merabia, S., & Hassanali, A. (2019). Thermal transport at a nanoparticle-water interface: A molecular dynamics and continuum modeling study. *The Journal of Chemical Physics*, *150*(11), 114701. https://doi.org/10.1063/1.5084234

Rubbi, F., Das, L., Habib, K., Aslfattahi, N., Saidur, R., & Rahman, M. T. (2021). State-of-the-art review on water-based nanofluids for low temperature solar thermal collector application. *Solar Energy Materials and Solar Cells*, *230*, 111220. https://doi.org/https://doi.org/10.1016/j.solmat.2021.111220

Rubbi, F., Habib, K., Saidur, R., Aslfattahi, N., Yahya, S. M., & Das, L. (2020). Performance optimization of a hybrid PV/T solar system using Soybean oil/MXene nanofluids as A new class of heat transfer fluids. *Solar Energy*, *208*, 124-138. https://doi.org/https://doi.org/10.1016/j.solener.2020.07.060

Safaei, M. R., Ahmadi, G., Goodarzi, M. S., Safdari Shadloo, M., Goshayeshi, H. R., & Dahari, M. (2016). Heat Transfer and Pressure Drop in Fully Developed Turbulent Flows of Graphene Nanoplatelets–Silver/Water Nanofluids. *Fluids*, *1*(3), 20. https://www.mdpi.com/2311-5521/1/3/20

Saikia, T., Mahto, V., & Kumar, A. (2017). Quantum dots: A new approach in thermodynamic inhibitor for the drilling of gas hydrate bearing formation. *Journal of Industrial and Engineering Chemistry*, *52*, 89-98. https://doi.org/https://doi.org/10.1016/j.jiec.2017.03.029

Samylingam, L., Aslfattahi, N., Saidur, R., Yahya, S. M., Afzal, A., Arifutzzaman, A., Tan, K. H., & Kadirgama, K. (2020). Thermal and energy performance improvement of hybrid PV/T system by using olein palm oil with MXene as a new class of heat transfer fluid. *Solar Energy Materials and Solar Cells*, *218*, 110754. https://doi.org/https://doi.org/10.1016/j.solmat.2020.110754

Sardarabadi, M., & Passandideh-Fard, M. (2016). Experimental and numerical study of metal-oxides/water nanofluids as coolant in photovoltaic thermal systems (PVT). *Solar Energy Materials and Solar Cells*, *157*, 533-542. https://doi.org/https://doi.org/10.1016/j.solmat.2016.07.008

Sardarabadi, M., Passandideh-Fard, M., & Zeinali Heris, S. (2014). Experimental investigation of the effects of silica/water nanofluid on PV/T (photovoltaic thermal units). *Energy*, *66*, 264-272. https://doi.org/https://doi.org/10.1016/j.energy.2014.01.102

Senthilraja, S., Vijayakumar, K. C. K., & Gangadevi, R. (2015). A COMPARATIVE STUDY ON THERMAL CONDUCTIVITY OF Al2O3/WATER, CuO/WATER AND Al2O3 - CuO/WATER NANOFLUIDS [Article]. *Digest Journal of Nanomaterials and Biostructures*, *10*(4), 1449-1458. <Go to ISI>://WOS:000369979800005

Součková, M., Klomfar, J., & Pátek, J. (2014). Measurements and group contribution analysis of 0.1MPa densities for still poorly studied ionic liquids with the [PF6] and [NTf2] anions. *The Journal of Chemical Thermodynamics*, *77*, 31-39. https://doi.org/https://doi.org/10.1016/j.jct.2014.04.017

Souza, R. R., Gonçalves, I. M., Rodrigues, R. O., Minas, G., Miranda, J. M., Moreira, A. L. N., Lima, R., Coutinho, G., Pereira, J. E., & Moita, A. S. (2022). Recent advances on the thermal properties and applications of nanofluids: From nanomedicine to renewable energies. *Applied Thermal Engineering*, *201*, 117725. https://doi.org/https://doi.org/10.1016/j.applthermaleng.2021.117725

Varmira, K., Baseri, M. M., Khanmohammadi, S., Hamelian, M., & Shahsavar, A. (2021). Experimental study of the effect of sheet-and-sinusoidal tube collector on the energetic and exergetic performance of a photovoltaic-thermal unit filled with biologically synthesized water/glycerol-silver nanofluid. *Applied Thermal Engineering*, *186*, 116518. https://doi.org/https://doi.org/10.1016/j.applthermaleng.2020.116518

Wanatasanappan, V. V., Abdullah, M. Z., & Gunnasegaran, P. (2020). Thermophysical properties of Al2O3-CuO hybrid nanofluid at different nanoparticle mixture ratio: An experimental approach. *Journal of Molecular Liquids*, *313*, 113458. https://doi.org/https://doi.org/10.1016/j.molliq.2020.113458

Yang, M., Diao, K., & Zhu, Y. (2022). Experimental investigation on mid-temperature thermal stability of WO2.9-SiC binary nanofluid. *Chemical Physics Letters*, *800*, 139655. https://doi.org/https://doi.org/10.1016/j.cplett.2022.139655